Targeted analysis of cell-free circulating tumor DNA is suitable for early relapse and actionable target detection in patients with neuroblastoma

Lodrini M., Graef J., Thole-Kliesch T.M., Astrahantseff K., Sprüssel A., Grimaldi M., Peitz C., Linke R.B., Hollander J.F., Lankes E., Künkele A., Oevermann L., Schwabe G., Fuchs J., Szymansky A., Schulte J.H., Hundsdoerfer P., Eckert C., Amthauer H., Eggert A., Deubzer H.E.

Clinical Cancer Research
2022 MAY 01 ; 28(9): 1809-1820
2022 FEB 22 (first published online)
doi: 10.1158/1078-0432.CCR-21-3716

Publisher: American Association for Cancer Research

Targeted analysis of cell-free circulating tumor DNA is suitable for early relapse and actionable target detection in patients with neuroblastoma

Marco Lodrini[1,2,3], Josefine Graef[4], Theresa M. Thole-Kliesch[1], Kathy Astrahantseff[1], Annika Sprüssel[1], Maddalena Grimaldi[1,2,3], Constantin Peitz[1,2,3], Rasmus B. Linke[1,2,3], Jan F. Hollander[1,2,3], Erwin Lankes[5,6], Annette Künkele[1,7], Lena Oevermann[1], Georg Schwabe[8], Jörg Fuchs[9], Annabell Szymansky[1], Johannes H. Schulte[1,7,10,11], Patrick Hundsdörfer[1,12], Cornelia Eckert[1], Holger Amthauer[3], Angelika Eggert[1,7,10,11], Hedwig E. Deubzer[1,2,3,7,10,11]

[1] Department of Pediatric Hematology and Oncology, Charité - Universitätsmedizin Berlin, Berlin, Germany
[2] Experimental and Clinical Research Center (ECRC) of the Charité and the Max-Delbrück-Center for Molecular Medicine (MDC) in the Helmholtz Association, Berlin, Germany
[3] Max-Delbrück-Center for Molecular Medicine (MDC) in the Helmholtz Association, Berlin, Germany
[4] Department of Nuclear Medicine, Charité - Universitätsmedizin Berlin, Berlin, Germany
[5] Department of Pediatric Endocrinology and Diabetes, Charité - Universitätsmedizin Berlin, Berlin, Germany
[6] Center for Chronically Sick Children, Charité - Universitätsmedizin Berlin, Berlin, Germany
[7] Berliner Institut für Gesundheitsforschung (BIH), Berlin, Germany
[8] Children's Hospital, Carl-Thiem-Klinikum, Cottbus, Germany
[9] Department of Pediatric Surgery and Paediatric Urology, University Children´s Hospital, Eberhard-Karls-University Tuebingen, Tuebingen, Germany
[10] German Cancer Consortium (DKTK), partner site Berlin, Berlin, Germany
[11] German Cancer Research Center (DKFZ), Heidelberg, Germany
[12] Department of Pediatric Oncology, Helios Klinikum Berlin Burch, Berlin, Germany

Running title: Longitudinal neuroblastoma disease monitoring using ctDNA

Corresponding author
PD Dr. Hedwig E. Deubzer, MD
Charité – Universitätsmedizin Berlin, Department of Pediatric Hematology and Oncology
Augustenburger Platz 1, 13353 Berlin, Germany
Phone: +49 30 450 616 157, E-mail: hedwig.deubzer@charite.de

Keywords: cancer, liquid biopsy, droplet digital PCR, *ALK*, *MYCN*, copy number variation, SNV, minimal residual disease, precision medicine, imaging

List of abbreviations: ALL, acute lymphoblastic leukemia; cfDNA, cell-free DNA; CNV, copy number variation; CSF, cerebrospinal fluid; ctDNA, circulating tumor DNA; ddPCR, droplet digital PCR; FDA, U.S. Food and Drug Administration; MIBG, ^{123}I-meta-iodobenzylguanidine; SNV, single-nucleotide variant

Article type: Research article
Conflict of interest: The authors have declared that no conflict of interest exists.

Financial Support: This work was supported by the Berlin Institute of Health (BIH) through the collaborative research consortium CRG-04 TERMINATE-NB to H.E.D., A.K., J.H.S. and A.E., through the Translational Oncology program of the German Cancer Aid within the consortium ENABLE (70112951) to H.E.D., A.K., J.H.S. and A.E, by the European Union and the Federal Ministry of Education and Research through the TRANSCAN-2 consortium LIQUIDHOPE (01KT1902) to H.E.D. and by the German Cancer Consortium (DKTK) partner site Berlin to M.L., A.E. and H.E.D. A.K. and H.E.D. are supported by the Advanced Clinician Scientist Program funded by the Charité – University Medicine Berlin and the BIH. A.E. and H.E.D. are members of the MSTARS consortium (161L0220A) financed through the Federal Ministry of Education and Research (BMBF) as part of the National Research Cores for Mass Spectrometry in Systems Medicine (MSCoreSys).

250-word structured abstract; 149-word statement of translational relevance
5,071 words of text, 53 references
6 figures, 6 supplementary figures, 14 supplementary tables

ABSTRACT

Purpose: Treating refractory or relapsed neuroblastoma remains challenging. Monitoring body fluids for tumor-derived molecular information indicating minimal residual disease supports more frequent diagnostic surveillance and may have the power to detect resistant subclones before they give rise to relapses. If actionable targets are identified from liquid biopsies, targeted treatment options can be considered earlier.

Experimental design: Droplet digital PCR assays assessing *MYCN* and *ALK* copy numbers and allelic frequencies of *ALK* p.F1174L and *ALK* p.R1275Q mutations were applied to longitudinally collected liquid biopsies and matched tumor tissue samples from 31 patients with high-risk neuroblastoma. Total cell-free DNA (cfDNA) levels and marker detection were compared with data from routine clinical diagnostics.

Results: Total cfDNA concentrations in blood plasma from patients with high-risk neuroblastoma were higher than in healthy controls and consistently correlated with neuron-specific enolase levels and lactate dehydrogenase activity but not with ^{123}I-meta-iodobenzylguanidine scores at relapse diagnosis. Targeted cfDNA diagnostics proved superior for early relapse detection to all current diagnostics in two patients. Marker analysis in cfDNA indicated intratumor heterogeneity for cell clones harboring *MYCN* amplifications and druggable *ALK* alterations that were not detectable in matched tumor tissue samples in 17 patients from our cohort. Proof-of-concept is provided for molecular target detection in cerebrospinal fluid from patients with isolated CNS relapses.

Conclusions: Tumor-specific alterations can be identified and monitored during disease course in liquid biopsies from pediatric patients with high-risk neuroblastoma. This approach to cfDNA surveillance warrants further prospective validation and exploitation for diagnostic purposes and to guide therapeutic decisions.

TRANSLATIONAL RELEVANCE

The invasive nature of surgical biopsies hinders their sequential application to monitor solid cancers. Single biopsies fail to reflect endogenous and treatment-driven cancer dynamics and clonal heterogeneity in the patient. We demonstrate that cell-free tumor DNA detection and marker surveillance in biofluids from patients with high-risk neuroblastoma provides molecular resolution of spatial and temporal disease activity superior to tissue-based diagnostics in individual patients. This minimally invasive liquid biopsy approach is applicable for the clinical routine. Monitoring disease is particularly important in this patient subgroup, in whom 50% experience relapse, who only <10% survive. Validation of our application for early molecular relapse diagnosis and monitoring minimal residual disease and druggable alterations (*MYCN* and *ALK* copy number, *ALK* p.F1174L and *ALK* p.R1275Q hotspot mutations) is warranted in large prospective studies for this rare cancer type to test if this liquid biopsy-based approach improves diagnostic power and translates into improved patient survival.

INTRODUCTION

The molecular landscape of solid tumors is currently assessed using DNA and/or RNA extracted from tissue samples. Endogenous and exogenous pressures, however, cause these molecular profiles to dynamically evolve over time. Competition among the heterogeneous genetic background of multiple subclonal populations and stress exerted on tumor cells by conventional cytotoxic chemotherapy and targeted therapies represent major processes driving tumor evolution (1). Increasing evidence suggests that recent technical advances improving sensitivity and accuracy of detection and characterization of total cell-free DNA (cfDNA), RNA and/or circulating tumor cells in liquid biopsies could allow clinicians to non-invasively monitor tumor evolution by multiple longitudinal testing (2). Liquid biopsy-based diagnostic approaches have begun to be incorporated into routine disease monitoring for the first cancer entities afflicting adult patients (3, 4). A large number of clinical trials currently evaluate circulating tumor DNA (ctDNA) diagnostics for further adult cancer entities, addressing a variety of observational and interventional research questions, including using liquid biopsy-based findings to prompt therapeutic actions (5). Liquid biopsy applications for pediatric oncology lag behind their adult counterpart, with predominantly retrospective proof-of-concept studies in small cohorts so far (6).

The pediatric tumor, neuroblastoma, originates from neuroectodermal progenitor cells and is the most frequent extracranial solid tumor in infancy and childhood (7). Approximately half of all newly diagnosed neuroblastomas are designated high-risk for relapse (8). Multimodal therapy including induction, surgery, high-dose chemotherapy followed by autologous stem cell rescue, radiation and anti-GD2 directed monoclonal antibody-based immunotherapy provokes a good initial response. However, minimal residual disease with few disseminated resistant tumor cells frequently causes tumors to relapse (9). Treating refractory or relapsed neuroblastoma remains challenging (10). Despite advances made in international efforts, minimal residual disease monitoring must be improved and therapy resistance must be

detected earlier at any time during therapy. Monitoring minimal residual disease in peripheral blood or bone marrow supports more frequent diagnostic surveillance and may have the power to detect chemotherapy-resistant clones before they leave the bone marrow niche, where they can arise even years after initial diagnosis. If actionable targets are identified in liquid biopsies used to monitor patients, second-line targeted treatment options could be considered much nearer to detecting therapy nonresponse.

That molecular features determine neuroblastoma aggressiveness and risk for relapse is well documented (10), adding *MYCN* amplifications and *ALK* mutations or amplifications, among others, to the clinical risk factors (11). Molecular factors have classically been assessed from the single diagnostic primary tumor biopsy. However, recent publications demonstrate clonal and subclonal heterogeneity in neuroblastomas at diagnosis (12) and branched clonal evolution with increasing molecular heterogeneity at relapse (13), supporting the necessity to monitor clonal evolution for optimal personalized care. These revelations may also explain why existing DNA- and mRNA-based molecular classifiers (14-16) do not sufficiently predict differential survival and heterogeneous outcomes in patients with high-risk disease. *MYCN* amplification occurs in approximately 25% of neuroblastomas and is a strong predictive biomarker for unfavorable patient survival (17). Recent data suggests *MYCN* amplification can exist at the (sub)clonal level, necessitating biosampling procedures and technologies capable of detecting these cell populations (18, 19). Activating mutations in the anaplastic lymphoma kinase (*ALK*) gene occur in 8% of neuroblastomas, the most frequent causing the F1174L and R1275Q substitutions in the receptor tyrosine kinase domain (20-23). ALK-driven neuroblastomas often develop relapses that may have expanded from a single *ALK* mutant clone (24) and are frequently resistant to chemo- and radiotherapy (9, 20, 21). Activating *ALK* mutations or amplifications have become the first target in neuroblastoma that is directly druggable by small molecule inhibitors as a personalized medicine approach

(25, 26), necessitating continuous molecular monitoring in patients with neuroblastoma for potential (re)emergence of *ALK* mutant or amplified clones.

Several studies most recently demonstrated that pediatric patients with solid tumors including neuroblastomas have blood ctDNA levels detectable with next-generation sequencing approaches (27-30). Optimized pre-analytical sample processing allowed reliable assessment of copy number variations, segmental chromosomal changes and single-nucleotide variants in ctDNA from children with neuroblastoma, hepatoblastoma and sarcoma (30, 31). Chicard and colleagues reported the feasibility of genomic copy number profiling of blood-based cfDNA from 70 patients with neuroblastoma using a molecular inversion probe-based OncoScan array (27). In a follow-up study, they combined whole-exome sequencing with deep-coverage targeted sequencing to investigate sequential liquid biopsy samples from 19 patients with neuroblastoma and characterize patterns of clonal evolution (28). Scientific laboratories across the globe including ours established multiplexed detection of *MYCN* and *ALK* amplifications and *ALK* hotspot mutations by droplet digital PCR (ddPCR) using total cfDNA purified from biofluids and genomic DNA extracted from tumor tissue as input materials (27, 30, 32-34). This study investigated the potential of monitoring ctDNA-based markers for advanced molecular longitudinal disease monitoring and actionable target identification using ddPCR protocols applicable for the routine clinical setting.

MATERIALS AND METHODS

Patient samples

Blood plasma, bone marrow plasma and cerebrospinal fluid (CSF) samples were collected together with matched formalin-fixed paraffin-embedded or snap frozen tumor samples (local ethics approval: EA2/055/17) from 31 patients with stage M, high-risk neuroblastoma according to the International Neuroblastoma Risk Group (11) (**Table 1**). Peripheral blood and bone marrow was uniformely collected in EDTA tubes without the addition of stabilizers.

CSF was sampled in sterile 10 ml polypropylene screw-cap tubes. Median patient age was 33.3 months [min-max: 2.1 – 169.0 months] (**Suppl. Table S1**). All patients were treated at the Charité – University Medicine Berlin and registered in the German NB2004 Trial (EudraCT 20661) or the NB 2016 Registry (**Suppl. Table S2**). Informed written patient/parent consent was obtained during trial/registry participation. White blood cells served as a source for germline DNA. Blood plasma was collected (local ethics approval: EA2/131/11) from 25 pediatric patients with non-malignant conditions and a median age of 72.4 months [min-max: 21.6 - 244.4 months] as comparative controls. Likewise, bone marrow plasma was collected (local ethics approval: EA4/132/17) from 24 healthy individuals with a median age of 23.2 years [min-max: 4.5 - 46.4 years]. Archived surplus bone marrow plasma from 28 pediatric patients with ALL collected at initial diagnosis was also investigated as a non-neuroblastoma control. All patients with ALL were treated within the AIEOP-BFM ALL 2009 (EudraCT 2007-004270-43) or AIEOP-BFM ALL 2017 trials (EudraCT 2016-001935-12) and had a median age of 5.7 years [min-max: 1.9 – 17.4 years]. Informed written patient/parent consent was obtained during trial participation. All studies involving human subjects were conducted in accordance with the Declaration of Helsinki. Peripheral blood and CSF were centrifuged at 1,900 x *g* for 7 min to separate plasma or remove cell debris (32). Bone marrow was centrifuged at 450 x *g* for 7 min to separate plasma from cells. The average time interval from collecting the blood, bone marrow or CSF sample to separating plasma or removing cell debris was 1 hour (inter-quartile range 0.5 – 1.9 hours). All plasma and CSF samples were centrifuged a second time at 3,250 x *g* for 10 min to remove cell debris before storage at -80 °C.

Response assessment to treatment

Overall response to treatment was assessed in line with revised International Neuroblastoma Response Criteria (35). In brief, overall response integrated tumor response in the primary

tumor, soft tissue, bone metastases and bone marrow. Primary and metastatic soft tissue sites were assessed using the Response Evaluation Criteria in Solid Tumors (RECIST) and ^{123}I-meta-iodobenzylguanidine (MIBG) imaging or ^{18}F-fluorodeoxyglucose positron emission magnetic resonance imaging (^{18}F-FDG-PET-MRI) for MIBG-nonavid tumors. Cytology and GD2 immunocytology were assessed in bone marrow cytospins. Tumor marker assessment was performed during routine clinical diagnostics and included blood levels of neuron-specific enolase, lactate dehydrogenase and ferritin as well as urine concentrations of the catecholamine metabolites, homovanillic acid and vanillylmandelic acid. Overall response was defined as complete, partial or minor response or stable or progressive disease (35).

Genomic and cell-free DNA preparation

Genomic DNA was extracted from tumor tissues using the Qiagen Puregene Core kit A (Qiagen) or the QIAamp DNA Mini kit (Qiagen) according to manufacturer's instructions, and quantified on a Qubit 2.0 fluorometer (Life Technologies). Fragmentation was achieved by 5U of AluI or HaeIII restriction enzyme (New England Biolabs) added to each ddPCR reaction (32). Thawed blood or bone marrow plasma and CSF samples were centrifuged at 2000 × *g* for 5 min to clear debris, then supernatants were centrifuged at 20,000 × *g* for 5 min. Cell-free DNA was purified from a minimum of 120 µl stored samples using the QIAamp Circulating Nucleic Acid kit (Qiagen), then concentrated to 50 µl using the DNA Clean and Concentrator-5 kit (Zymo Research), both according to manufacturers' directions. Total cfDNA was quantified using the cell-free DNA ScreenTape assay (Agilent) and Agilent 4200 TapeStation System according to manufacturer's instructions (33). DNA fragments between 100 – 300 bp were considered to be total cfDNA (36). The total cfDNA amount available for further analysis is summarized in **Suppl. Table S3** for the different study populations. In total, 2.3% of all samples subjected to ddPCR contained a DNA input amount insufficient for a clear assay result.

Droplet digital PCR

The QX200 Droplet Digital PCR System (Bio-Rad) was used to determine *MYCN* (2p24.3) and *ALK* (2p23.2-2p23.1) copy number and detect *ALK* p.F1174L (3522, C>A) and *ALK* p.R1275Q (3824, G>A) hotspot mutations with their corresponding wildtype sequences in duplex ddPCR assays as previously described (32, 33). Amplification of either the *MYCN* or *ALK* gene was defined as detecting ≥ 8.01 gene copies by ddPCR analysis, while 2.74 to 8.00 copies indicated a gene gain and 1.50 to 2.73 copies indicated the normal diploid gene contingent (32). In the background of plasma, 1 ng ctDNA is required to reliably quantify tumor-specific copy number alterations. This limit of detection was determined by spiking 0.01 – 10 ng of sonicated genomic DNA from six neuroblastoma cell lines with varying *MYCN* amplification levels into plasma from pediatric patients with non-malignant conditions (**Suppl. Fig. S1**). Briefly, the following T100 Thermo Cycler (Bio-Rad) programs were performed: (i) CNV: denaturation at 95°C for 10min, 40 cycles of 30sec at 94°C and 1min at 58°C and final denaturation for 10min 98°C and (ii) SNV: denaturation at 95°C for 10min, 40 cycles of 30sec at 94°C and 1min at 62.5°C and final denaturation for 10min 98°C. Optimized primer and probe concentrations for CNVs and SNVs are summarized in **Suppl. Tables S4** and **S5**, respectively. Target gene CNV and mutant allele frequency were analyzed using QuantaSoft Analysis software, version 1.7.4.0917 (Bio-Rad). All ddPCR assays contained appropriate non-template, positive and negative controls in each run to enable software to generate specific thresholds. The QuantaSoft Analysis software used for duplex ddPCR assays determined copy number by calculating the ratio of target molecule concentration, A (copies/µl), to the reference molecule concentration, B (copies/µl), times the number of reference species copies, $N_{B,}$ in the human genome ($copy\ number = \frac{A}{B} \times N_B$).False positive rate and limit of detection for SNV analyses were calculated with Bio-Rad lookup tables in line with the model by Armbruster and Pry (37). False positive rate was, in principle,

calculated from two parameters, the number of false-positive droplets and the minimally required concentration of mutant target molecules. False positive rate calculation was performed for each SNV protocol as described (33). A sample was scored as positive if both the number of droplets detecting the respective mutation and the concentration of mutant target molecules (copies/µl) were above the set thresholds (33).

Statistical analysis

The non-parametric Mann-Whitney U test evaluated the significance of differences between total cfDNA concentrations in patient cohorts. The statistical relationship between two variables was calculated using Pearson's correlation coefficient. All tests were conducted using GraphPad Prism version 7.0 (GraphPad Software) *P*-values below 0.05 were considered significant.

Data availability

Targeted sequencing data have been deposited into the European Genome-phenome Archive under accession number EGAS00001006027 (https://www.ebi.ac.uk/ega/home). Original ddPCR data generated in this study are available upon request from the corresponding author.

RESULTS

Cell-free DNA is detectable in body fluids from patients with high-risk neuroblastoma

Circulating cfDNA was previously reported to be present at higher levels in blood plasma from patients with cancer compared to healthy individuals (38). We set out to validate this in blood plasma collected at initial and/or relapse diagnosis prior to starting systemic therapy in 31 patients with high-risk neuroblastoma (**Suppl. Tables S1** and **S2**). Control blood plasma samples were available as residues from routine endocrinological diagnostics from 25 children. Median cfDNA levels were 68-fold higher in blood plasma from patients with high-risk neuroblastoma compared to controls at initial diagnosis (**Fig. 1A**). Similarly, cfDNA

levels in blood plasma from patients with high-risk neuroblastoma at relapse diagnosis were 5-fold higher compared to controls (**Fig. 1A**). The concentration of circulating cfDNA varied considerably more at initial diagnosis than at diagnosis of relapse in the study cohort, and the median total cfDNA concentration at initial diagnosis was 13-fold higher than at relapse diagnosis (**Fig. 1A**). Segregating the study cohort according to the age at diagnosis, the tumor *MYCN*-, chromosome 1p36- or *ALK* status demonstrated no differences in total cfDNA concentration (**Fig. 1B** and **Suppl. Fig. S2**). We next compared cfDNA concentrations purified from bone marrow plasma collected from healthy individuals or pediatric patients at initial diagnosis of ALL or high-risk neuroblastoma with infiltrated bone marrow. Bone marrow-derived cfDNA concentrations in patient groups with neuroblastoma and ALL were similar, and on average up to 5-fold higher compared to controls (**Fig. 1C**). A comparison of blood and bone marrow-derived cfDNA levels demonstrated a strong correlation between both compartments, suggesting either a high correlation between systemic disease burden and disease activity in the bone marrow niche or a pre-analytical dilution of the bone marrow through peripheral blood during the sampling process (**Fig. 1D**). Additional data sets including single-cell analyses from the bone marrow niche are necessary to reliably interpret ctDNA surveillance from bone marrow plasma and its clinical diagnostic potential. We performed a data meta-analysis to investigate the relationship between cfDNA amount shed into peripheral blood and established parameters for disease activity, cellular turnover and systemic disease burden from blood (neuron-specific enolase, lactate dehydrogenase activity and ferritin), urine (the catecholamine metabolites, homovanillic acid and vanillylmandelic acid) and the scoring results from diagnostic ^{123}I-meta-iodobenzylguanidine imaging. These analyses demonstrated that cfDNA levels in patients with high-risk neuroblastoma closely correlated at both initial and relapse diagnosis with neuron-specific enolase levels and lactate dehydrogenase activity but not with ferritin levels or catecholamine metabolite excretion in the urine (**Fig. 2A-B**, **Suppl. Fig. S3**). MIBG-derived Curie scores (39) correlated with total

cfDNA in blood plasma at initial diagnosis but not diagnosis of relapse (**Fig. 2C**). MIBG scores according to SIOPEN (40) correlated with blood plasma cfDNA levels at initial diagnosis in the bone compartment but not in any other constellation (**Fig. 2D**). Altogether, total cfDNA concentrations are higher in blood and bone marrow plasma from patients with high-risk neuroblastoma than in healthy controls, and the extent of ctDNA shed into the blood most closely correlated with markers for neuronal activity and high cellular turnover.

Targeted ctDNA profiling captures intratumor heterogeneity

Multi-region tumor sequencing has shown that the multiple genomic aberrations detected vary within the tumor, demonstrating intratumor heterogeneity (41). Clonal evolution of mutations and copy numbers was also recently reported in neuroblastomas (42). To test whether ctDNA-based diagnostics can detect intratumor heterogeneity not reflected in single biopsies, we compared marker profiles in matched blood and tumor tissue samples. The first blood sample collected from each patient at initial and/or relapse diagnosis was used for comparison, demonstrating that *MYCN* copy number was generally strongly correlated between cfDNA and tumor tissue (**Fig. 3A**, **Suppl. Table S6**). In two patients, a tumor *MYCN* amplification or gain were not detected in cfDNA purified from the first blood sample collected (**Fig. 3A**, **Suppl. Tables S7** and **S8**). In one patient, a tumor *MYCN* amplification was detected as a gain in cfDNA (**Fig. 3A**), most likely due to dilution of the high-level *MYCN* copy number signal through background DNA signals released from healthy tissues into circulation. Strikingly, cfDNA analysis detected a *MYCN* amplification in three patients classified as tumor *MYCN* diploid (**Fig. 3A**; one of these cases exemplarily shown in **Suppl. Fig. S4A** and **Suppl. Table S9**). Similarly, a *MYCN* amplification was detected in cfDNA from two patients whose tumor analysis detected a *MYCN* gain. This data indicates that cfDNA analysis detected *MYCN*-amplified tumor clones or subclones not reflected in the tumor biopsy used to characterize molecular disease. Comparing *ALK* copy number in cfDNA and tumor tissue produced a similar picture. A tumor *ALK* gain was not detected in the first blood sample from four patients, but detected in subsequent samples (**Fig. 3B**, **Suppl. Table S6**). Vice versa, an *ALK* gain was measured in cfDNA that was not detected in the tumor samples available from 13 patients at initial and/or relapse diagnosis (**Fig. 3B**). Detection of *ALK* p.F1174L and *ALK* p.R1275Q hotspot mutations were strongly concordant between cfDNA and tumor tissue. Tumor mutant allele frequencies were below 1% in 3 patients, and not detectable in cfDNA purified from the first blood sample collected (**Fig. 3C-D**, **Suppl.**

Table S6). In one of these cases, the *ALK* p.F1174L mutation became detectable in all follow-up blood samples (**Suppl. Fig. S4A**, **Suppl. Table S9**). The *ALK* p.R1275Q mutation detected in cfDNA from one patient was neither detected in the initial tumor biopsy nor resected tumor tissue from this patient (**Fig. 3D**). Altogether, these findings support that neuroblastoma in a patient is spatially genetically heterogeneous and that this clonal heterogeneity is reflected in circulating cfDNA. This finding has implications for *ALK* inhibitor therapy selection.

Blood-based ctDNA analysis enables molecular neuroblastoma relapse detection

We next evaluated whether disease could be longitudinally monitored in blood and bone marrow plasma collected from patients with high-risk neuroblastoma during treatment course. Molecular analysis of tumor tissue from patient B50 identified a *MYCN* amplification and an *ALK* gain (**Suppl. Fig. S5A**, **Suppl. Table S7**). Both markers were employed to retrospectively analyze *MYCN* and *ALK* CNVs in blood and bone marrow plasma collected during induction chemotherapy, surgery, high-dose chemotherapy followed by autologous stem cell rescue and immunotherapy (**Fig. 4A**). INRC response assessment determined a complete remission in patient B50 on day 220 after admission to the Charité (**Fig. 4A**). Likewise, *MYCN* and *ALK* copy numbers in blood-derived cfDNA were normal (**Fig. 4A**). On day 247, 6 copies of the *MYCN* amplicon were detected in blood-derived cfDNA while *ALK* copy numbers remained normal (**Fig. 4A**). Routine restaging on day 350 in the patient (clinically inapparent disease) revealed an MIBG-positive relapse localized to two independent sites in lower extremity bones (**Fig. 4A**). A biopsy obtained from one lesion contained *MYCN*-amplified and *ALK*-diploid neuroblastoma cells (**Suppl. Fig. S5A**, **Suppl. Table S7**). An overall increase in cfDNA levels was observed in parallel, which was in line with median blood cfDNA levels in patients at relapse diagnosis (**Fig. 4A**). *MYCN* copy numbers further increased to 15, and three copies of the *ALK* gene were detected (**Fig. 4A**). While standard bone marrow diagnostics detected no active disease, cfDNA purified from

bone marrow plasma detected between 6 and 11 *MYCN* copies (**Fig. 4A**). Follow-up analysis on day 364 showed that *MYCN* copy numbers had increased to 26 in blood-derived cfDNA (**Fig. 4A**). Patient B50 reached a second complete remission through relapse therapy, and *MYCN* copy numbers normalized over time (**Suppl. Table S7**).

Targeted sequencing of the primary tumor from patient B22 demonstrated a partial *ALK* gain with approximately 4 copies (**Suppl. Fig. S5B**). This finding was utilized to retrospectively analyze blood- and bone marrow-derived cfDNA from this patient. The first sample was collected during routine follow-up after first-line treatment, when patient B22 had been in persistent first remission for 15.7 months, and revealed diploid *ALK* status and a comparatively high cfDNA level (**Fig. 4B, Suppl. Table S10**). The next follow-up sample, collected 10 days later, detected three *ALK* copies (**Fig. 4B**). Routine follow-up diagnostics performed on day 122 showed a relapse in the primary tumor region. Molecular analysis of biopsied tumor tissue collected on day 134 demonstrated persistence of the *ALK* gain (**Suppl. Fig. S5B**), and blood-derived cfDNA from day 132 confirmed the *ALK* gain (**Fig. 4B**). Patient B22 also reached a second complete remission, and *ALK* copy numbers normalized during relapse treatment (**Suppl. Table S10**). Radiographic evidence of relapse lagged 102 and 122 days behind ctDNA-based relapse detection in patients B50 and B22, respectively. Hence, targeted cfDNA diagnostics proved superior to all clinically established approaches for early relapse detection in two patients with high-risk neuroblastoma in our cohort.

Rapid clearance of ctDNA markers is contrasted by marker persistence in patients with the most divergent outcomes

We retrospectively longitudinally monitored two patients with high-risk neuroblastoma, who responded well to induction treatment and were in complete remission at the time of publication. Molecular analysis of tumor tissue identified a *MYCN* amplification and an *ALK* p.R1275Q mutation in patient B10 (**Fig. 5A**, **Suppl. Table S11**) and a *MYCN* amplification

and an *ALK* p.F1174L mutation in patient B42 (**Fig. 5B**, **Suppl. Table S12**). Retrospective marker analysis in blood- and bone marrow-derived cfDNA longitudinally collected from both patients during therapy showed a molecular remission prior to day 100 of induction therapy in the liquid biopsy compartments, while standard imaging demonstrated active disease in a metastatic lesion (patient B10) and the primary tumor (patient B42), retrospectively (**Fig. 5A-B**). Whether rapid ctDNA tumor marker clearance correlates with favorable event-free survival will require prospective validation studies in large patient cohorts. The observation of rapid ctDNA marker clearance is contrasted by the sustained persistence of such markers in patients with refractory relapsed disease as exemplarily shown for patient B9. Molecular analysis of tumor tissue from patient B9 documented an *ALK* gain, which was consistently detected in blood- and bone marrow-derived cfDNA during second- and third-line treatment (**Suppl. Fig. S4B**, **Suppl. Table S13**). These findings demonstrate that therapy success is reflected in cfDNA-based longitudinal patient monitoring, but also that molecular markers are rapidly cleared from the blood after a patient responds well to treatment.

CSF-derived ctDNA analysis enables molecular monitoring of neuroblastoma relapse

We analyzed molecular markers in blood plasma and CSF derived from patient B35, who experienced neuroblastoma relapse in the central nervous system between the fourth and fifth immunotherapy cycle. Tumor tissue was *MYCN*-amplified at initial diagnosis (**Suppl. Fig. S6**), when > 8 *MYCN* copies were detected with high total cfDNA levels in blood (**Fig. 6**). Standard diagnostics documented complete remission prior to high-dose chemotherapy, and *MYCN* cfDNA levels normalized (**Fig. 6**). At relapse, a *MYCN* amplification was detected in tumor tissue and CSF-derived cfDNA (**Fig. 6**, **Suppl. Fig. S6**). Following neurosurgical intervention and start of intrathecal and systemic relapse treatment, *MYCN* copy numbers in the CSF dropped to normal diploid levels (**Fig. 6**). Analysis of blood- and bone marrow-

derived cfDNA detected normal *MYCN* copy numbers at all time points except day four after neurosurgical intervention. At this time point, four *MYCN* cfDNA copies were detected, which may reflect manipulation associated with the surgical intervention (**Fig. 6**; **Suppl. Table S14**). Patient B35 reached a second remission that was associated with reduced cfDNA levels in the CSF to below detection thresholds. We provide proof-of-concept that molecular targets can be detected in CSF from patients with neuroblastoma.

DISCUSSION

Here we provide proof-of-principle that liquid biopsy-based targeted approaches employing ddPCR can be used for disease monitoring in patients with high-risk neuroblastoma. Circulating cfDNA in blood plasma contains representative neuroblastoma-derived genetic material capturing common genetic alterations in the *MYCN* and *ALK* oncogenes. This ctDNA surveillance retrospectively identified high-risk neuroblastoma relapses in patients with no other evidence of disease during consolidation therapy (patient B50, marker: amplified *MYCN*) or after primary treatment with curative intent during follow-up (patient B22, marker: *ALK* gain). This suggests that identifying recurrence in patients with no clinical, radiological or currently routine tumor marker-based evidence of disease may become a key use of liquid biopsies in patients with high-risk neuroblastoma. Recurrences were identified with a median of 3.5 months before clinical evidence of disease, in line with ctDNA surveillance in patients with diffuse large B-cell lymphoma (43) and colorectal cancer (44). This is the first study documenting the superiority of cfDNA-based diagnostics using nonpatient-specific ddPCR assays for early molecular relapse detection in patients with high-risk neuroblastoma. Whether a switch to proactive second-line “rescue” therapies based on early detection of molecular relapse or insufficient first-line response can improve overall survival for patients with high-risk neuroblastoma remains to be investigated. However, studies on minimal

residual disease activity in leukemias have sustainably changed management of these diseases (45) hinting at the potential of ctDNA surveillance for high-risk neuroblastoma.

Several studies demonstrate that CSF is also suitable to analyze ctDNA in patients with primary brain tumors, including high-grade glioma and medulloblastomas (46), and tumors metastasized to the brain (47). Only low ctDNA levels circulate in blood from these individuals, possibly due to the blood-brain barrier (46). In line with a previous case report employing a quantitative real-time PCR approach (48), we demonstrate that *MYCN* amplification can be detected in cfDNA purified from the CSF from a patient with an isolated leptomeningeal/intracerebral neuroblastoma relapse (patient B35). This patient received repeated intrathecal topotecan administered via a CSF reservoir, allowing longitudinal CSF collection for *MYCN* copy number analysis. *MYCN* copy number decreased over time with response to therapy, suggesting that CSF-based ctDNA can be used to monitor patients with neuroblastoma CNS relapses. This is interesting because the number of neuroblastoma CNS relapses is expected to increase in coming years, since immunotherapies such as the GD2-targeting monoclonal antibody cannot cross the blood-brain barrier, and this highly vulnerable patient population remains challenging to treat. *MYCN* amplification was detected in parallel in blood-based ctDNA from patient B35, with this signal also decreasing over time to reach normal values when secondary complete remission was achieved. Neurosurgery may, at least in part, have enabled the blood-based signal by disturbing the blood-brain barrier or the signal may have come primarily from the leptomeningeal relapse components. Proximity of neuroblastoma brain metastases to the cortical surface, in direct contact to the CSF, may also influence ctDNA shedding into this compartment and signal strength in ctDNA surveillance. Monitoring in further patients treated for neuroblastoma CNS relapses could illuminate the physiology behind ctDNA target source during surveillance in CSF and blood plasma to improve interpretation of ctDNA surveillance of CNS-metastasized disease. Genomic methodologies such as the ddPCR assays used in this study particularly make applications in

clinical settings with pediatric patients, where only very low cfDNA levels are present, possible and have been shown to outperform classical quantitative real-time PCR approaches (49).

It is widely accepted that tumor type, location, cell turnover, vascularity and the presence and extent of circulating tumor cells and metastatic lesions influence blood ctDNA levels (46). In line with previous publications (27, 50), baseline characterization of total cfDNA in peripheral blood from patients at initial or relapse diagnosis of high-risk neuroblastoma prior to initiation of systemic therapy demonstrated significantly higher cfDNA levels than blood from healthy pediatric controls. The cfDNA concentrations detected, however, varied strongly among patients, and longitudinal total plasma cfDNA monitoring performed so far does not support a major role for total cfDNA monitoring for diagnostic neuroblastoma surveillance. Importantly, both *MYCN*/*ALK* CNVs and *ALK* SNVs could be identified even in samples yielding the lowest cfDNA levels.

Single tissue biopsies do not fully mirror the spatial heterogeneity of stage M neuroblastoma as metastatic lesions are per se only very rarely biopsied. This study demonstrates that liquid biopsy-based diagnostics contributes to the identification of aggressive neuroblastoma cell clones harboring oncogenic gene amplifications or mutations that are not reflected in the tumor tissues available for molecular analysis. Specifically, the data suggests that neuroblastoma cell clones harboring alterations in the *MYCN* and *ALK* oncogenes are overrepresented in circulating tumor cells and/or metastases at distant sites. This observation supports a model in which neuroblastoma cells driven by MYCN and/or ALK are prone to migrate to and invade distant sites, thus, pointing towards intratumor heterogeneity and underlining the role of activated MYCN and ALK signaling pathway for neuroblastoma aggressiveness (20-23). In accordance with this model, this study also reports the co-detection of *ALK* p.F1174L and *ALK* p.R1275Q mutations in plasma samples, but only the *ALK* p.F1174L mutation in the tumor tissue. The codetection of two *ALK* hotspot mutations in

blood plasma but not the biopsy specimen from a patient with neuroblastoma has been previously reported (34), supporting clinical decision-making for targeted ALK inhibitor therapy based on ctDNA diagnostics. Altogether, this study identified genetic alterations exclusively in the ctDNA but not in tumor DNA in 10% of the patient cohort, which presents a novel finding compared to previous studies employing ddPCR approaches to study ctDNA (27, 30, 34).

The comparative analysis of *ALK* hotspot mutations in matched liquid biopsy-tumor tissue samples also demonstrates that mutant allele frequencies below 1% in tumor tissue are not detected in ctDNA diagnostics. This may be due to a very small amount of circulating tumor material, which is below the sensitivity threshold of the ddPCR technology applied. *MYCN* and *ALK* copy number assessment in matched liquid biopsies and tumor tissue samples revealed loss of oncogene gain detection in the ctDNA diagnostics in few samples, most likely due to dilution effects mediated by background from DNA released from normal cells (51). Both observations highlight the importance of matched liquid biopsy-tumor tissue studies to capture the complete spectrum of genomic alterations driving malignancy through complementary analyses. The overall high concordance for *MYCN* and *ALK* copy numbers and *ALK* p.F1174L and *ALK* p.R1275 allelic frequencies between blood-based ctDNA and tumor tissue in our patient cohort is in line with the mutational profiles detected in the *KRAS*, *NRAS*, *PIK3CA*, *BRAF* and *EGFR* oncogenes in matched blood-based ctDNA-tumor tissue samples from patients with breast (46), colorectal (52) and lung cancer (53). Altogether, a plasma-positive test in the presence of tissue negativity is most likely due to the failure of the single tissue biopsy to capture the intratumor heterogeneity of metastasized disease, and presents a strong argument for implementing dual tissue-plasma testing in patients with neuroblastoma.

The clinical potential for liquid biopsy-based molecular surveillance is just beginning to be appreciated for early diagnosis, prognostication and identifying molecular relapses as well as

assessing therapy response, secondary drug resistance or minimal residual disease. Here we demonstrate that ddPCR-based ctDNA surveillance in liquid biopsies is applicable in the routine clinical setting and suitable for molecular profiling, early relapse detection and actionable target identification in pediatric patients with high-risk neuroblastoma. Validation studies based on standard operating procedures for liquid biopsy sampling are warranted to test pre-analytical feasibility in the multi-center setting and define the potential of ctDNA diagnostics for future interventional trials.

ACKNOWLEDGEMENTS

The authors thank the patients and their parents, who agreed to take part in this study, and Daniela Tiburtius, Jasmin Wünschel, Jutta Proba, Constanze Passenheim and Nadine Sachs for excellent technical assistance.

AUTHOR CONTRIBUTIONS

Conceptualization: M. Lodrini, A. Eggert, H.E. Deubzer. **Data curation**: M. Lodrini, M. Grimaldi, C. Peitz, J.F. Hollander. **Formal analysis**: M. Lodrini, J. Graef, T.M. Thole, A. Sprüssel, C. Peitz, A. Szymansky, C. Eckert, H. Amthauer, H.E. Deubzer. **Supervision:** M. Lodrini, H. Amthauer, A. Eggert, H.E. Deubzer. **Validation:** M. Lodrini, H.E. Deubzer. **Investigation:** M. Lodrini, M. Grimaldi, C. Peitz, R.B. Linke, J.F. Hollander, A. Szymansky, H.E. Deubzer. **Visualization:** M. Lodrini, K. Astrahantseff, H.E. Deubzer. **Methodology:** M. Lodrini, J. Graef, A. Sprüssel, C. Peitz. **Writing-original draft:** M. Lodrini, K. Astrahantseff, A. Eggert, H.E. Deubzer. **Project administration:** M. Lodrini, H.E. Deubzer. **Resources:** T.M. Thole, E. Lankes, A. Künkele, L. Oevermann, G. Schwabe, J. Fuchs, JH Schulte, P. Hundsdörfer, C. Eckert, H.E. Deubzer. **Funding acquisition:** H.E. Deubzer.

REFERENCES

1. McGranahan N, Swanton C. Clonal Heterogeneity and Tumor Evolution: Past, Present, and the Future. Cell. 2017;168:613-28.
2. Siravegna G, Marsoni S, Siena S, Bardelli A. Integrating liquid biopsies into the management of cancer. Nature Rev Clin Oncol. 2017;14:531-48.
3. Luo J, Shen L, Zheng D. Diagnostic value of circulating free DNA for the detection of EGFR mutation status in NSCLC: a systematic review and meta-analysis. Sci Rep. 2014;4:6269.
4. Andre F, Ciruelos E, Rubovszky G, Campone M, Loibl S, Rugo HS, et al. Alpelisib for PIK3CA-Mutated, Hormone Receptor-Positive Advanced Breast Cancer. New Engl J Med. 2019;380:1929-40.
5. Siravegna G, Mussolin B, Venesio T, Marsoni S, Seoane J, Dive C, et al. How liquid biopsies can change clinical practice in oncology. Ann Oncol; 2019;30:1580-90.
6. Van Paemel R, Vlug R, De Preter K, Van Roy N, Speleman F, Willems L, et al. The pitfalls and promise of liquid biopsies for diagnosing and treating solid tumors in children: a review. Eur J Pediatr. 2020;179:191-202.
7. Brodeur GM. Neuroblastoma: biological insights into a clinical enigma. Nature Rev Cancer. 2003;3:203-16.
8. Park JR, Eggert A, Caron H. Neuroblastoma: biology, prognosis, and treatment. Hematol Oncol Clin North Am. 2010;24:65-86.
9. Maris JM. Recent advances in neuroblastoma. New Engl J Med. 2010;362:2202-11.
10. Matthay KK, Maris JM, Schleiermacher G, Nakagawara A, Mackall CL, Diller L, et al. Neuroblastoma. Nature Rev Dis Primers. 2016;2:16078.
11. Monclair T, Brodeur GM, Ambros PF, Brisse HJ, Cecchetto G, Holmes K, et al. The International Neuroblastoma Risk Group (INRG) staging system: an INRG Task Force report. J Clin Oncol. 2009;27:298-303.
12. Boeva V, Popova T, Bleakley K, Chiche P, Cappo J, Schleiermacher G, et al. Control-FREEC: a tool for assessing copy number and allelic content using next-generation sequencing data. Bioinformatics. 2012;28:423-5.
13. Schramm A, Koster J, Assenov Y, Althoff K, Peifer M, Mahlow E, et al. Mutational dynamics between primary and relapse neuroblastomas. Nat Genet. 2015;47:872-7.
14. Janoueix-Lerosey I, Schleiermacher G, Michels E, Mosseri V, Ribeiro A, Lequin D, et al. Overall genomic pattern is a predictor of outcome in neuroblastoma. J Clin Oncol. 2009;27:1026-33.
15. De Preter K, Vermeulen J, Brors B, Delattre O, Eggert A, Fischer M, et al. Accurate outcome prediction in neuroblastoma across independent data sets using a multigene signature. Clin Cancer Res. 2010;16(5):1532-41.
16. Oberthuer A, Hero B, Berthold F, Juraeva D, Faldum A, Kahlert Y, et al. Prognostic impact of gene expression- based classification for neuroblastoma. J Clin Oncol. 2010;28:3506-15.
17. Brodeur GM, Seeger RC, Schwab M, Varmus HE, Bishop JM. Amplification of N-myc in untreated human neuroblastomas correlates with advanced disease stage. Science. 1984;224:1121-4.
18. Marrano P, Irwin MS, Thorner PS. Heterogeneity of MYCN amplification in neuroblastoma at diagnosis, treatment, relapse, and metastasis. Genes Chromosomes Cancer. 2017;56:28-41.
19. Berbegall AP, Bogen D, Potschger U, Beiske K, Bown N, Combaret V, et al. Heterogeneous MYCN amplification in neuroblastoma: a SIOP Europe Neuroblastoma Study. Br J Cancer. 2018;118:1502-12.
20. Mosse YP, Laudenslager M, Longo L, Cole KA, Wood A, Attiyeh EF, et al. Identification of ALK as a major familial neuroblastoma predisposition gene. Nature. 2008;455:930-5.
21. Janoueix-Lerosey I, Lequin D, Brugieres L, Ribeiro A, de Pontual L, Combaret V, et al. Somatic and germline activating mutations of the ALK kinase receptor in neuroblastoma. Nature. 2008;455:967-70.
22. Chen Y, Takita J, Choi YL, Kato M, Ohira M, Sanada M, et al. Oncogenic mutations of ALK kinase in neuroblastoma. Nature. 2008;455:971-4.
23. George RE, Sanda T, Hanna M, Frohling S, Luther W, 2nd, Zhang J, et al. Activating mutations in ALK provide a therapeutic target in neuroblastoma. Nature. 2008;455:975-8.
24. Schleiermacher G, Javanmardi N, Bernard V, Leroy Q, Cappo J, Rio Frio T, et al. Emergence of new ALK mutations at relapse of neuroblastoma. J Clin Oncol. 2014;32:2727-34.
25. Mosse YP, Lim MS, Voss SD, Wilner K, Ruffner K, Laliberte J, et al. Safety and activity of crizotinib for paediatric patients with refractory solid tumours or anaplastic large-cell lymphoma: a Children's Oncology Group phase 1 consortium study. Lancet Oncol. 2013;14:472-80.
26. Sekimizu M, Osumi T, Fukano R, Koga Y, Kada A, Saito AM, et al. A Phase I/II Study of Crizotinib for Recurrent or Refractory Anaplastic Lymphoma Kinase-Positive Anaplastic Large Cell Lymphoma and a Phase I Study of Crizotinib for Recurrent or Refractory Neuroblastoma: Study Protocol for a Multicenter Single-arm Open-label Trial. Acta Med Okayama. 2018;72:431-6.

27. Chicard M, Boyault S, Colmet Daage L, Richer W, Gentien D, Pierron G, et al. Genomic Copy Number Profiling Using Circulating Free Tumor DNA Highlights Heterogeneity in Neuroblastoma. Clin Cancer Res. 2016;22:5564-73.
28. Chicard M, Colmet-Daage L, Clement N, Danzon A, Bohec M, Bernard V, et al. Whole-Exome Sequencing of Cell-Free DNA Reveals Temporo-spatial Heterogeneity and Identifies Treatment-Resistant Clones in Neuroblastoma. Clin Cancer Res. 2018;24:939-49.
29. Klega K, Imamovic-Tuco A, Ha G, Clapp AN, Meyer S, Ward A, et al. Detection of Somatic Structural Variants Enables Quantification and Characterization of Circulating Tumor DNA in Children With Solid Tumors. JCO Precis. Oncol. 2018;2018.
30. Kahana-Edwin S, Cain LE, McCowage G, Darmanian A, Wright D, Mullins A, et al. Neuroblastoma Molecular Risk-Stratification of DNA Copy Number and ALK Genotyping via Cell-Free Circulating Tumor DNA Profiling. Cancers. 2021;13.
31. Gerber T, Taschner-Mandl S, Saloberger-Sindhoringer L, Popitsch N, Heitzer E, Witt V, et al. Assessment of pre-analytical sample handling conditions for comprehensive liquid biopsy analysis. J Mol Diagn. 2020;22:1070-86.
32. Lodrini M, Sprussel A, Astrahantseff K, Tiburtius D, Konschak R, Lode HN, et al. Using droplet digital PCR to analyze MYCN and ALK copy number in plasma from patients with neuroblastoma. Oncotarget. 2017;8:85234-51.
33. Peitz C, Sprussel A, Linke RB, Astrahantseff K, Grimaldi M, Schmelz K, et al. Multiplexed Quantification of Four Neuroblastoma DNA Targets in a Single Droplet Digital PCR Reaction. J Mol Diagn. 2020.
34. Combaret V, Iacono I, Bellini A, Brejon S, Bernard V, Marabelle A, et al. Detection of tumor ALK status in neuroblastoma patients using peripheral blood. Cancer Med. 2015;4:540-50.
35. Park JR, Bagatell R, Cohn SL, Pearson AD, Villablanca JG, Berthold F, et al. Revisions to the International Neuroblastoma Response Criteria: A Consensus Statement From the National Cancer Institute Clinical Trials Planning Meeting. J Clin Oncol. 2017;35:2580-7.
36. Fan HC, Blumenfeld YJ, Chitkara U, Hudgins L, Quake SR. Noninvasive diagnosis of fetal aneuploidy by shotgun sequencing DNA from maternal blood. Proc Natl Acad Sci U S A. 2008;105:16266-71.
37. Armbruster DA, Pry T. Limit of blank, limit of detection and limit of quantitation. Clin Biochem Rev. 2008;29 Suppl 1:S49-52.
38. Siravegna G, Bardelli A. Genotyping cell-free tumor DNA in the blood to detect residual disease and drug resistance. Genome Biol. 2014;15:449.
39. Yanik GA, Parisi MT, Shulkin BL, Naranjo A, Kreissman SG, London WB, et al. Semiquantitative mIBG scoring as a prognostic indicator in patients with stage 4 neuroblastoma: a report from the Children's oncology group. J Nucl Med. 2013;54:541-8.
40. Lewington V, Lambert B, Poetschger U, Sever ZB, Giammarile F, McEwan AJB, et al. (123)I-mIBG scintigraphy in neuroblastoma: development of a SIOPEN semi-quantitative reporting method by an international panel. Eur J Nucl Med Mol Imaging. 2017;44:234-41.
41. Gerlinger M, Rowan AJ, Horswell S, Math M, Larkin J, Endesfelder D, et al. Intratumor heterogeneity and branched evolution revealed by multiregion sequencing. New Engl J Med. 2012;366:883-92.
42. Schmelz K, Toedling J, Huska M, Cwikla MC, Kruetzfeldt L-M, Proba J, et al. Spatial and temporal intratumour heterogeneity has potential consequences for single biopsy-based neuroblastoma treatment decisions. Nat Commun. 2021;12(1):6804.
43. Roschewski M, Dunleavy K, Pittaluga S, Moorhead M, Pepin F, Kong K, et al. Circulating tumour DNA and CT monitoring in patients with untreated diffuse large B-cell lymphoma: a correlative biomarker study. Lancet Oncol. 2015;16:541-9.
44. Diehl F, Schmidt K, Choti MA, Romans K, Goodman S, Li M, et al. Circulating mutant DNA to assess tumor dynamics. Nature Med. 2008;14:985-90.
45. Eckert C, Groeneveld-Krentz S, Kirschner-Schwabe R, Hagedorn N, Chen-Santel C, Bader P, et al. Improving Stratification for Children With Late Bone Marrow B-Cell Acute Lymphoblastic Leukemia Relapses With Refined Response Classification and Integration of Genetics. J Clin Oncol. 2019;37:3493-506.
46. Bettegowda C, Sausen M, Leary RJ, Kinde I, Wang Y, Agrawal N, et al. Detection of circulating tumor DNA in early- and late-stage human malignancies. Sci Transl Med. 2014;6:224ra24.
47. Pan W, Gu W, Nagpal S, Gephart MH, Quake SR. Brain tumor mutations detected in cerebral spinal fluid. Clin Chem. 2015;61:514-22.
48. Kimoto T, Inoue M, Tokimasa S, Yagyu S, Iehara T, Hosoi H, et al. Detection of MYCN DNA in the cerebrospinal fluid for diagnosing isolated central nervous system relapse in neuroblastoma. Pediatr Blood Cancer. 2011;56:865-7.
49. Diaz LA, Jr., Bardelli A. Liquid biopsies: genotyping circulating tumor DNA. J Clin Oncol. 2014;32:579-86.
50. Kurihara S, Ueda Y, Onitake Y, Sueda T, Ohta E, Morihara N, et al. Circulating free DNA as non-invasive diagnostic biomarker for childhood solid tumors. J Pediatr Surg. 2015;50:2094-7.

51. Snyder MW, Kircher M, Hill AJ, Daza RM, Shendure J. Cell-free DNA Comprises an In Vivo Nucleosome Footprint that Informs Its Tissues-Of-Origin. Cell. 2016;164:57-68.
52. Siravegna G, Mussolin B, Buscarino M, Corti G, Cassingena A, Crisafulli G, et al. Clonal evolution and resistance to EGFR blockade in the blood of colorectal cancer patients. Nature Med. 2015;21:827.
53. Fernandez-Cuesta L, Perdomo S, Avogbe PH, Leblay N, Delhomme TM, Gaborieau V, et al. Identification of Circulating Tumor DNA for the Early Detection of Small-cell Lung Cancer. EBioMedicine. 2016;10:117-23.

Fig. 1. Total cfDNA in plasma from blood and bone marrow is higher in patients with high-risk neuroblastoma than in healthy control individuals. Cell-free DNA concentrations are shown for blood plasma samples from patients with high-risk neuroblastoma (collected at the indicated times) and pediatric controls (**A**) and in the same patient cohort segregated according to presence of a tumor *MYCN* amplification (**B**). **C**, Cell-free DNA concentrations are shown for plasma from bone marrow samples collected from the patients in our cohort with bone marrow infiltration at initial diagnosis of high-risk neuroblastoma, healthy individuals and patients with acute lymphoblastic leukemia at diagnosis. Box-and-whisker plots indicate the median, interquartile range and minimum/maximum. Single data points are visualized as dots. $^{*}P \leq 0.05$; $^{**}P \leq 0.01$; $^{***}P \leq 0.001$; n.s., not significant. **D**, Correlation analysis between the cfDNA concentrations in blood and bone marrow plasma from high-risk neuroblastoma patients. Number of samples (n), Pearson's correlation coefficient (r) and *P*-value are indicated.

Fig. 2. Correlation analysis between tumor markers, MIBG scores and cfDNA concentration in blood plasma from patients with high-risk neuroblastoma. Significant correlations of cfDNA concentration in blood plasma versus neuron specific enolase (NSE) levels (**A**) and lactate dehydrogenase (LDH) activity are shown (**B**). Significant and non-significant correlations of cfDNA concentration in blood plasma versus ^{123}I-meta-iodobenzylguanidine scintigraphy (MIBG) scores according to Curie (**C**) and SIOPEN are shown (**D**). Number of samples (n), Pearson's correlation coefficient (r) and *P*-value are indicated.

Fig. 3. Comparison of four neuroblastoma DNA targets in tumor tissue and blood-based cfDNA. *MYCN* (**A**) and *ALK* (**B**) copy number status as well as *ALK* p.F1174L (**C**) and *ALK* p.R1275Q mutant allele frequencies (**D**) were quantified by ddPCR using genomic and cfDNA as input materials. Genomic DNA was isolated from biopsy and resection tumor tissue at initial and/or relapse diagnosis. For comparison, the first blood sample collected at initial and/or relapse diagnose from each patient was selected. The yellow colored sections indicate concordant results in tumor tissue and blood.

Fig. 4. Longitudinal disease monitoring by targeted copy number profiling of cfDNA detects molecular relapses of high-risk neuroblastoma. *MYCN* (green) and *ALK* (blue) copy numbers (detected by ddPCR in purified cfDNA, *upper time line*), total cfDNA concentrations (*lower time line*) and selected clinical case information (*below time lines*) are shown for longitudinally collected samples (type and times indicated in the graphical display) from patients B50 (**A**) and B22 (**B**). Total cfDNA concentrations of the selected samples were quantified using the Agilent 4200 TapeStation System. Dashed lines indicate the median cfDNA concentrations in the cohorts indicated. Light blue and white backgrounds represent different treatments modules. HDCT, high-dose chemotherapy; NDD, no detectable disease; RECIST, response evaluation criteria in solid tumors; RIST, molecularly targeted multimodal approach consisting of metronomic courses of rapamycin/dasatinib and irinotecan/temozolomide; S, surgery. INRC, International Neuroblastoma Response Criteria: CR, complete remission; MR, minor response; PD, progressive disease; PR, partial response; SD, stable disease.

Fig. 5. Clearance of cfDNA-based disease markers during induction therapy. *MYCN* copy number status (green), *ALK* p.F1174L (dark blue) and *ALK* p.R1275Q (blue) mutant allele frequencies (detected by ddPCR in purified cfDNA and genomic DNA, *upper time line*), total cfDNA concentrations (*lower time line*) and selected clinical case information (*below time lines*) are shown for longitudinally collected samples (type and times indicated in the graphical display) from patients B10 (**A**) and B42 (**B**). Total cfDNA concentrations of the selected samples were quantified using the Agilent 4200 TapeStation System. Dashed lines indicate the median cfDNA concentrations in the cohorts indicated. Light blue and white backgrounds represent different treatments modules. ALKi, ALK inhibitor treatment; DD, detectable disease; haplo SCT, haploidentical hematopoietic stem cell transplantation; HDCT, high-dose chemotherapy; MAF, mutant allele frequency; NDD, no detectable disease; ϟ, radiation; S, surgery. INRC, International Neuroblastoma Response Criteria: CR, complete remission; MR, minor response; PR, partial response; SD, stable disease.

Fig. 6. *MYCN* copy number assessment in cfDNA from cerebrospinal fluid enables monitoring of relapsed intracerebral/leptomeningeal neuroblastoma. *MYCN* copy numbers (detected by ddPCR in purified cfDNA, *upper time line*), total cfDNA concentrations (*lower time line*) and selected clinical case information (*below time lines*) are shown for longitudinally collected samples (type and times indicated in the graphical display) from patient B35. Total cfDNA concentrations of the selected samples were quantified using the Agilent 4200 TapeStation System. Dashed lines indicate the median cfDNA concentrations in the cohorts indicated. Light blue and white backgrounds represent different treatments modules. CNS, central nervous system; CSF, cerebrospinal fluid; DD, detectable disease; haplo SCT, haploidentical hematopoietic stem cell transplantation, HDCT, high-dose chemotherapy; I/T/DIN/G-CSF, irinotecan/temozolomide/dinutuximab beta/granulocyte colony stimulating factor; i.t., intrathecal; NDD, no detectable disease; RECIST, response evaluation criteria in solid tumors; ϟ,

radiation; S, surgery. INRC, International Neuroblastoma Response Criteria: CR, complete remission; PD, progressive disease; PR, partial response.

Figure 1

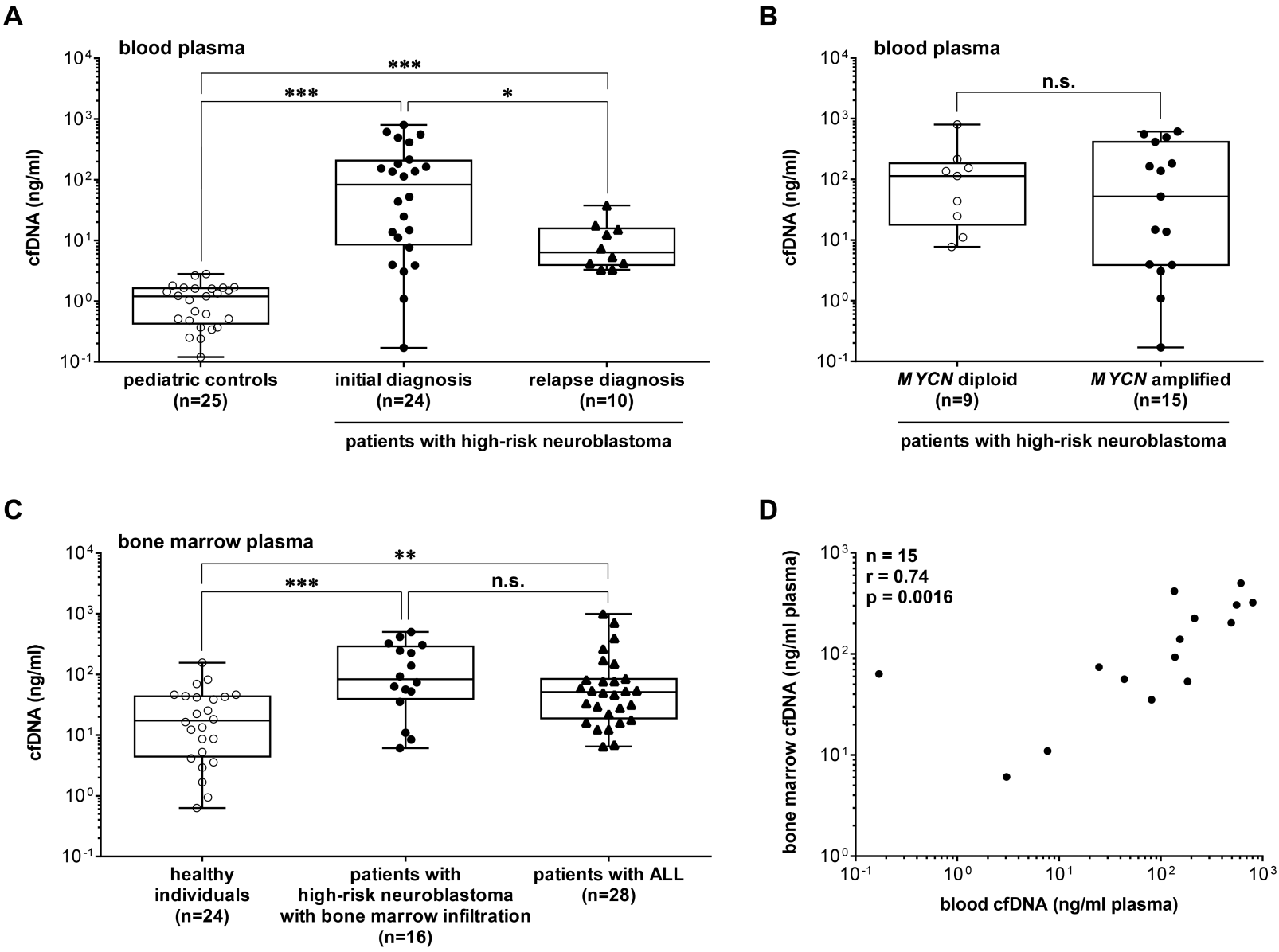
A
blood plasma
cfDNA (ng/ml)
***
***
*
pediatric controls (n=25)
initial diagnosis (n=24)
relapse diagnosis (n=10)
patients with high-risk neuroblastoma
B
blood plasma
cfDNA (ng/ml)
n.s.
MYCN diploid (n=9)
MYCN amplified (n=15)
patients with high-risk neuroblastoma
C
bone marrow plasma
cfDNA (ng/ml)
**
***
n.s.
healthy individuals (n=24)
patients with high-risk neuroblastoma with bone marrow infiltration (n=16)
patients with ALL (n=28)
D
n = 15
r = 0.74
p = 0.0016
bone marrow cfDNA (ng/ml plasma)
blood cfDNA (ng/ml plasma)

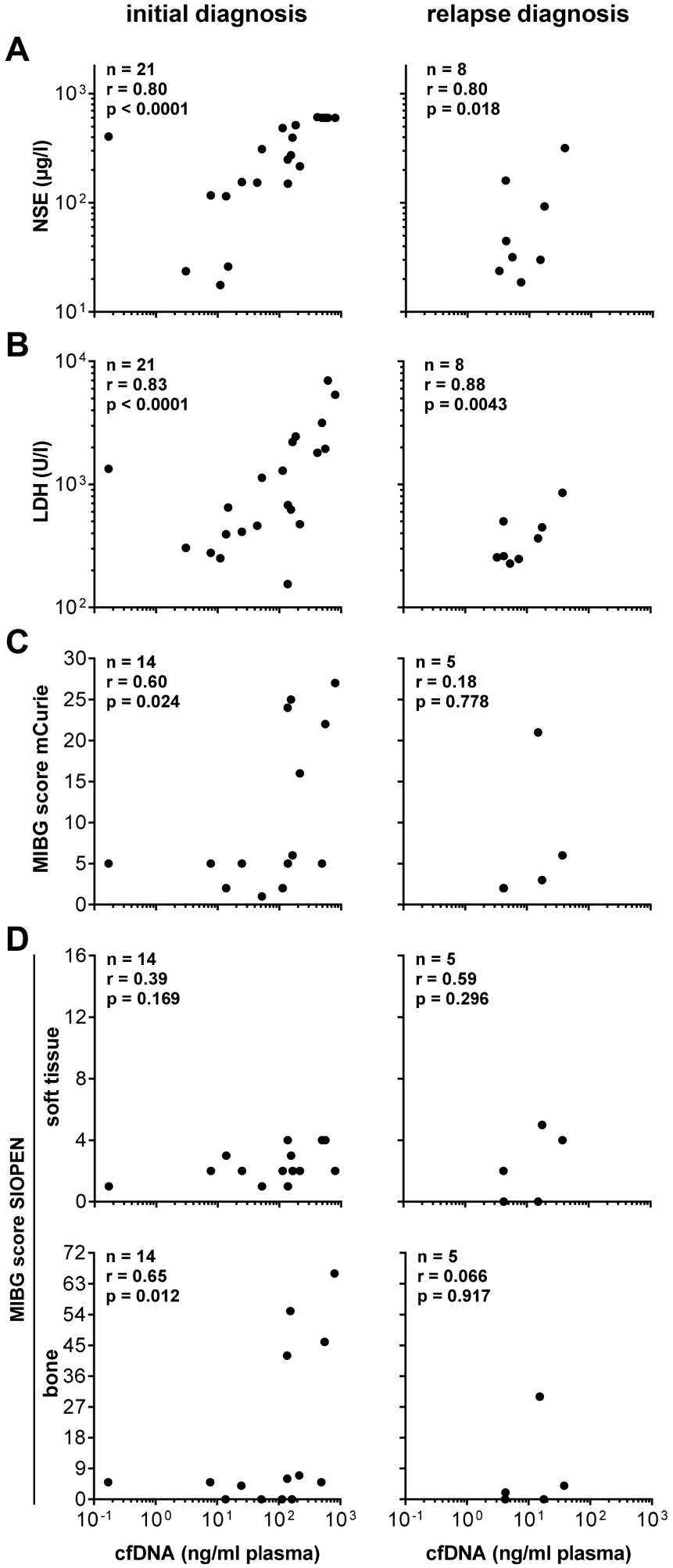
initial diagnosis
relapse diagnosis
A
n = 21
r = 0.80
p < 0.0001
n = 8
r = 0.80
p = 0.018
NSE (µg/l)
B
n = 21
r = 0.83
p < 0.0001
n = 8
r = 0.88
p = 0.0043
LDH (U/l)
C
n = 14
r = 0.60
p = 0.024
n = 5
r = 0.18
p = 0.778
MIBG score mCurie
D
MIBG score SIOPEN
soft tissue
n = 14
r = 0.39
p = 0.169
n = 5
r = 0.59
p = 0.296
bone
n = 14
r = 0.65
p = 0.012
n = 5
r = 0.066
p = 0.917
cfDNA (ng/ml plasma)
cfDNA (ng/ml plasma)

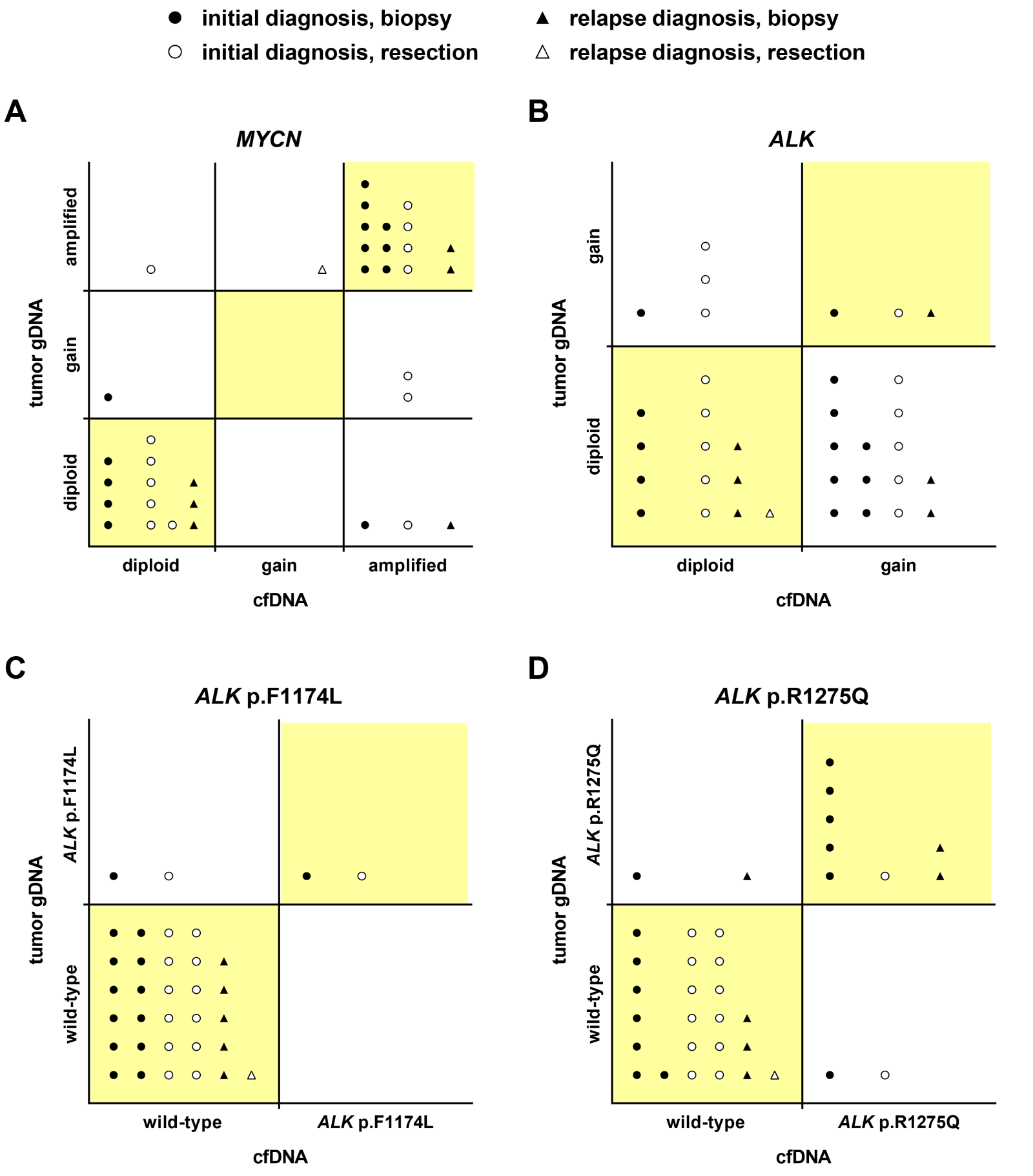
initial diagnosis, biopsy
initial diagnosis, resection
relapse diagnosis, biopsy
relapse diagnosis, resection
A
MYCN
amplified
gain
diploid
tumor gDNA
diploid
gain
amplified
cfDNA
B
ALK
gain
diploid
tumor gDNA
diploid
gain
cfDNA
C
ALK p.F1174L
ALK p.F1174L
wild-type
tumor gDNA
wild-type
ALK p.F1174L
cfDNA
D
ALK p.R1275Q
ALK p.R1275Q
wild-type
tumor gDNA
wild-type
ALK p.R1275Q
cfDNA

A

patient B50

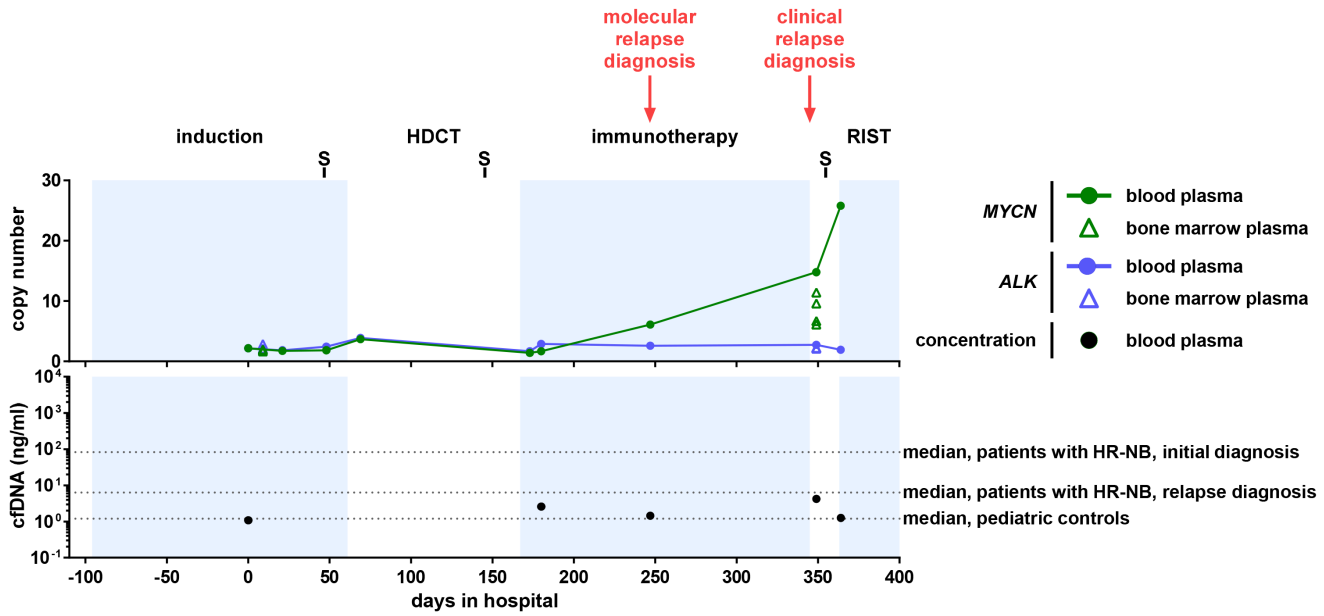

standard bone marrow diagnostics		NDD			NDD
response primary tumor		PR	CR	CR	CR
response metastasis		SD	PR	CR	PD
response INRC		MR	PR	CR	PD
MIBG score SIOPEN					
soft tissue (max. 16)	2	2	2	0	0
bone (max. 72)	7	0	0	0	2
MIBG score mCurie (max. 30)	9	2	2	0	2

B

patient B22

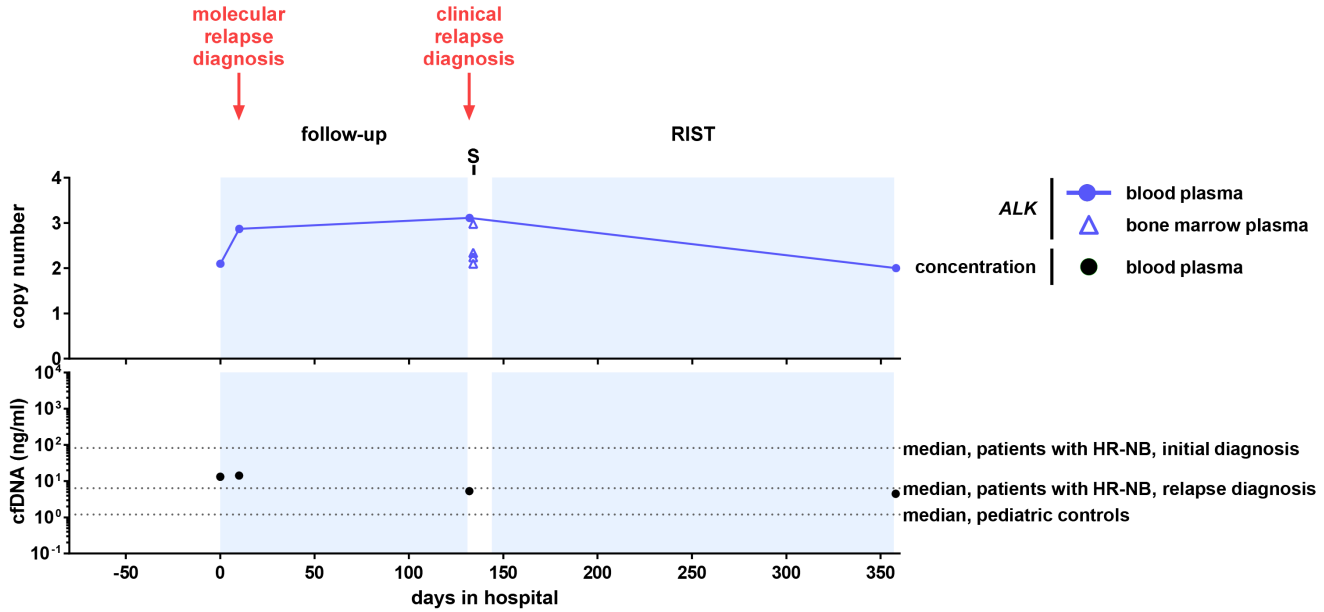

standard bone marrow diagnostics		NDD	
response primary tumor		CR	
response metastasis		PD	
response INRC		PD	
MIBG score SIOPEN			
soft tissue (max. 16)		2	
bone (max. 72)		0	
MIBG score mCurie (max. 30)		2	
RECIST	CR	PD	CR

Lodrini *et al.*

Figure 5

patient B35

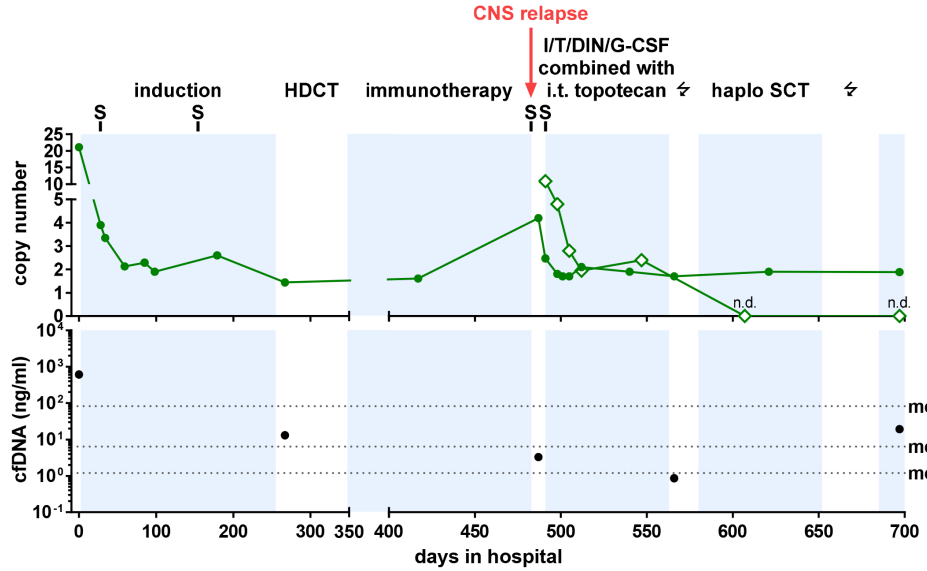

standard CSF diagnostics			NDD	NDD	NDD	NDD
standard bone marrow diagnostics	DD		NDD			
response primary tumor		PR	CR			
response metastasis		CR	PD			
response INRC		PR	PD			
RECIST		PR	CR	PD PR	CR	CR

A

patient B10

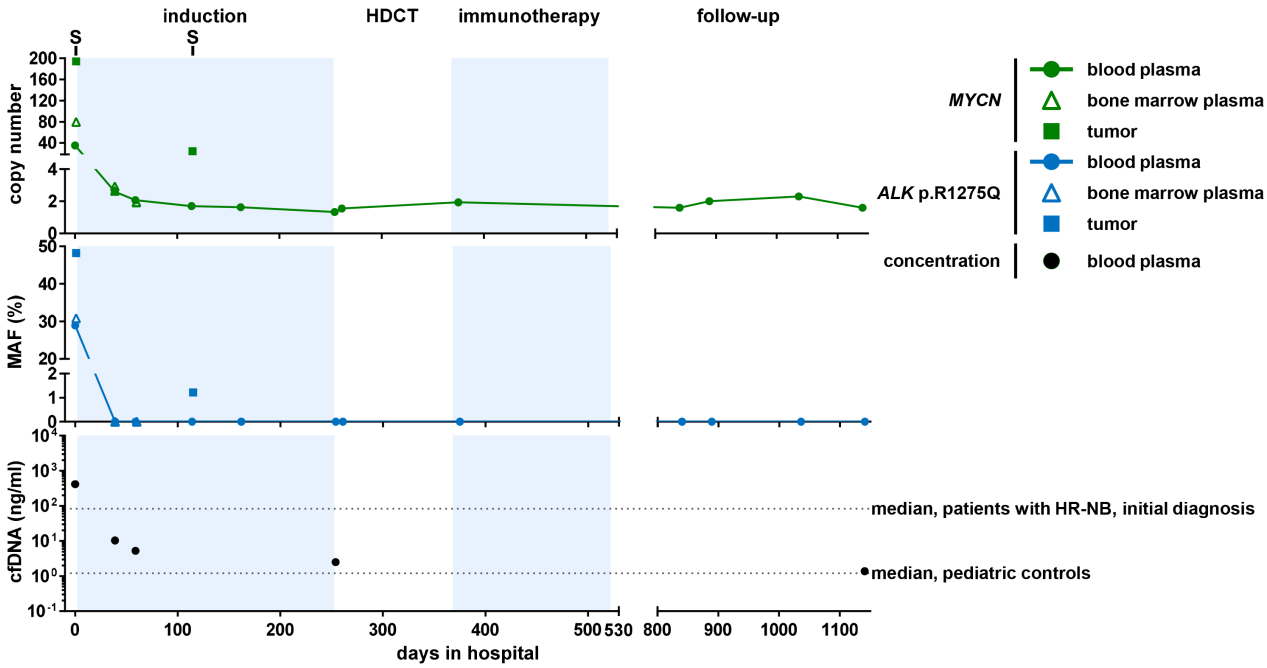

standard bone marrow diagnostics	DD	NDD		NDD	
response primary tumor		CR	CR	CR	CR
response metastasis		PR	CR	CR	CR
response INRC		PR	CR	CR	CR
MIBG score SIOPEN					
soft tissue (max. 16)	2	2	0	0	0
bone (max. 72)	0	0	0	0	0
MIBG score mCurie (max. 30)	2	2	0	0	0

B

patient B42

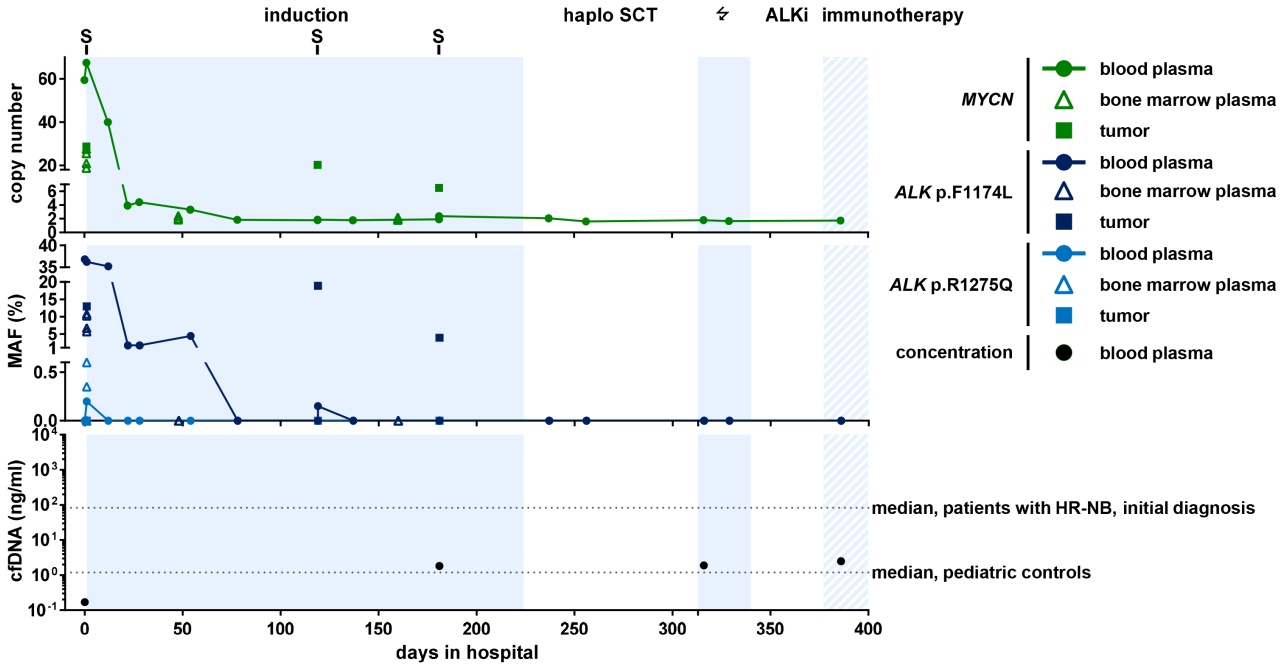

standard bone marrow diagnostics	DD	NDD		NDD	
response primary tumor		SD	SD	PR	CR
response metastasis		CR	CR	CR	CR
response INRC		MR	MR	PR	CR
MIBG score SIOPEN					
soft tissue (max. 16)	1	1	1	1	0
bone (max. 72)	5	0	0	0	0
MIBG score mCurie (max. 30)	5	1	1	1	0

SUPPLEMENTARY DATA

Targeted analysis of circulating tumor DNA is suitable for early relapse and actionable target detection in patients with neuroblastoma

Marco Lodrini, Josefine Graef, Theresa M. Thole-Kliesch, Kathy Astrahantseff, Annika Sprüssel, Maddalena Grimaldi, Constantin Peitz, Rasmus B. Linke, Jan F. Hollander, Erwin Lankes, Annette Künkele, Lena Oevermann, Georg Schwabe, Jörg Fuchs, Annabell Szymansky, Johannes H. Schulte, Patrick Hundsdörfer, Cornelia Eckert, Holger Amthauer, Angelika Eggert, Hedwig E. Deubzer

Table of Contents

SUPPLEMENTARY MATERIALS AND METHODS

Hybrid capture-based panel sequencing

Fresh-frozen tumor material was histologically evaluated by an experienced pathologist, and only regions with at least 10% tumor cell content were macrodissected. DNA was automatically extracted using a Maxwell Instrument (Promega), then sheared mechanically by ultrasonic acoustic energy (Covaris) before subjecting 100-200ng to a custom *NB* hybrid capture-based next-generation sequencing panel assay (NEO New Oncology GmbH) for neuroblastoma to detect point mutations, small insertions deletions, copy number alterations and rearrangement/gene fusions in a single assay (1). Adapters were ligated to sheared sample DNA, and individual genomic regions of interest were enriched using complementary bait sequences (hybrid capture procedure). Selected baits ensured optimal coverage of all relevant genomic regions. After enrichment, targeted fragments were amplified (clonal amplification) and sequenced in parallel with an average mean sequencing depth of 1000-2500x (unfiltered reads) (2). Data were analyzed using the NEO New Oncology custom analysis pipeline that assessed quality of the raw sequencing reads then aligned reads to the GRCh37 (hg19) human reference genome assembly (1). Discordant read pairs were subsequently extracted, and the structural variants and their breakpoints were localized. Positions of all detected alterations were recorded with all supporting data evidence (spanning and encompassing sequencing reads).

SUPPLEMENTARY FIGURES

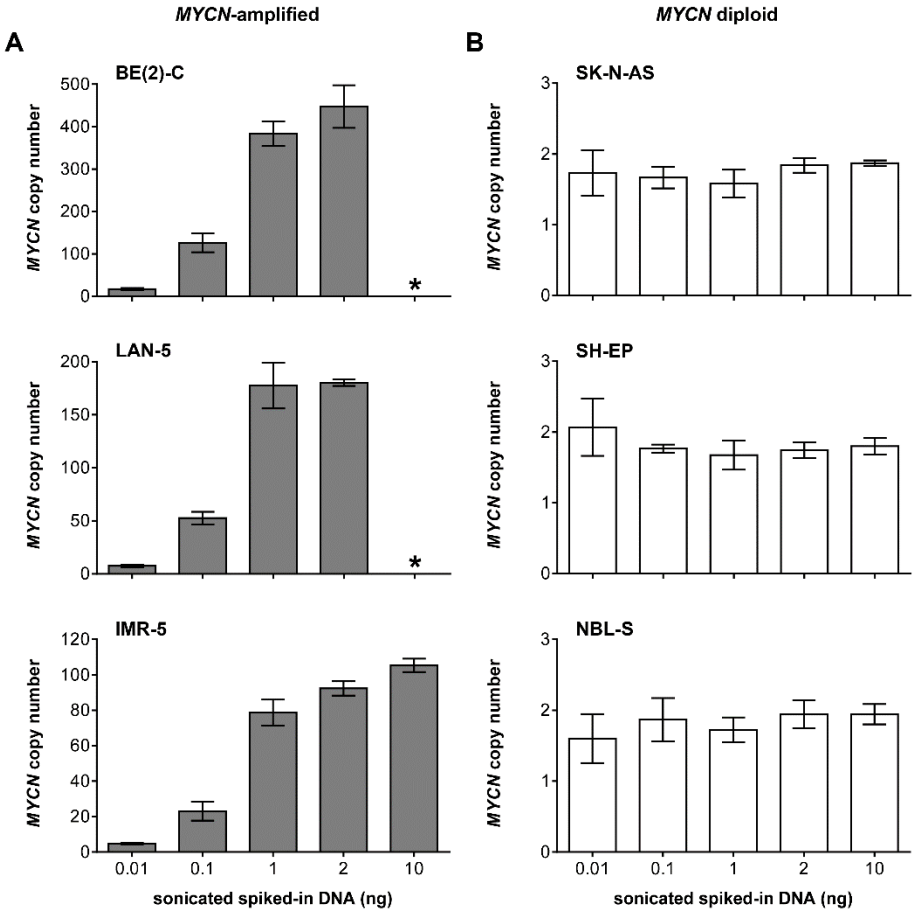

Suppl. Fig. S1. Limit of detection analysis for copy number alterations in circulating cell-free DNA. Sonicated genomic DNA from three *MYCN*-amplified (**A**) and three *MYCN* diploid neuroblastoma cell lines (**B**) was spiked in varying amounts (0.01 – 10 ng) into pooled plasma from pediatric patients with non-malignant conditions. *MYCN* copy number was assessed by ddPCR. *Saturated ddPCR reaction requiring re-analysis with lower input material.

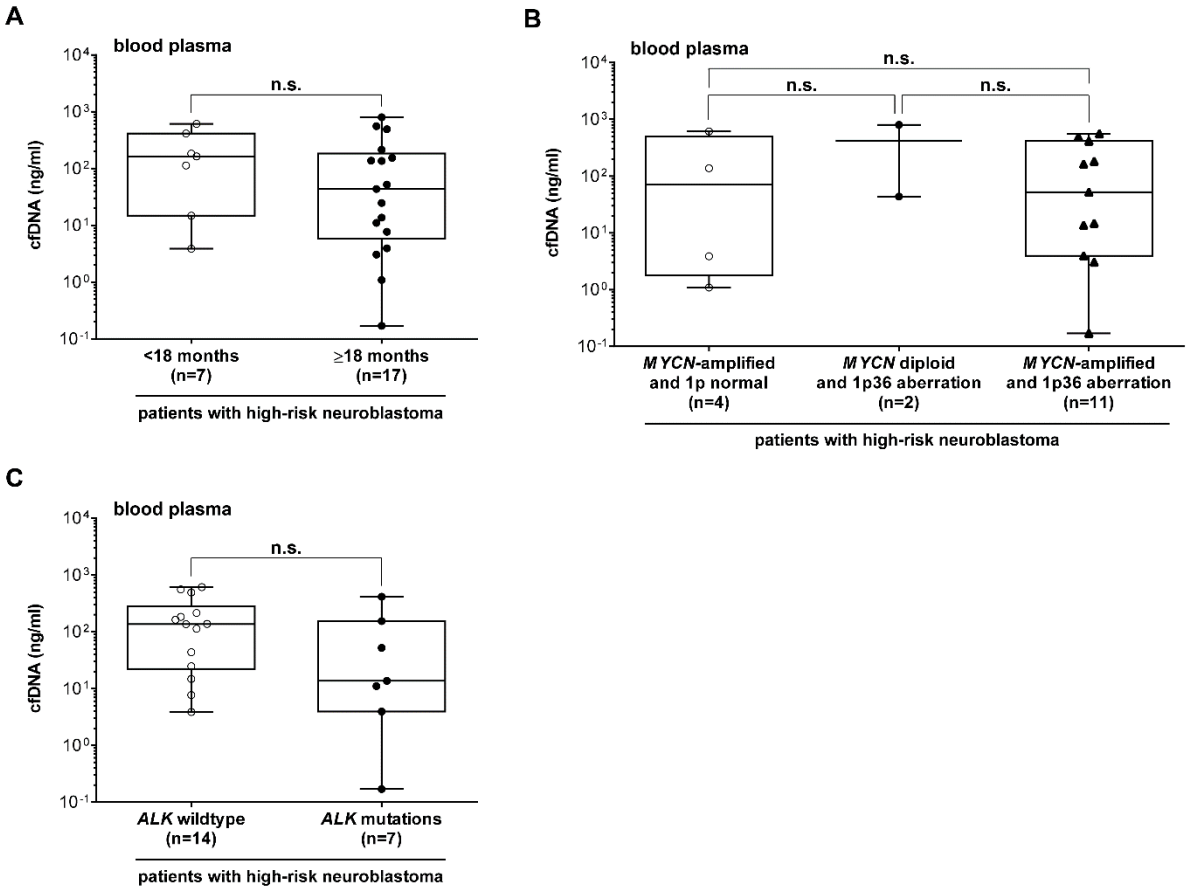

Suppl. Fig. S2. Comparison of total cfDNA concentrations in plasma from patients with high-risk neuroblastoma according to clinical and molecular risk factors. Cell-free DNA concentrations are shown for blood plasma samples from patients with high-risk neuroblastoma segregated according to the age at diagnosis (A) and the molecular marker constellation in tumor tissue (B, C). n.s., not significant.

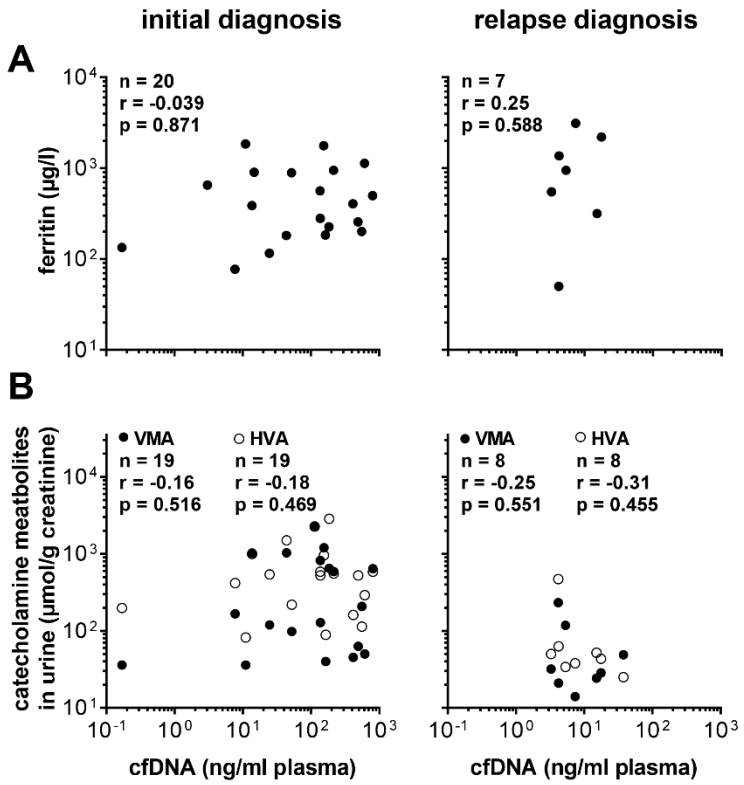

Suppl. Fig. S3. Correlation analysis between tumor markers and cfDNA concentration in blood plasma from patients with high-risk neuroblastoma. Non-significant correlations of cfDNA concentration in blood plasma versus blood ferritin levels (**A**) and catecholamine metabolites in urine are shown (**B**). Number of samples (n), Pearson's correlation coefficient (r) and *P*-value are indicated. HVA, homovanillic acid; VMA, vanillylmandelic acid.

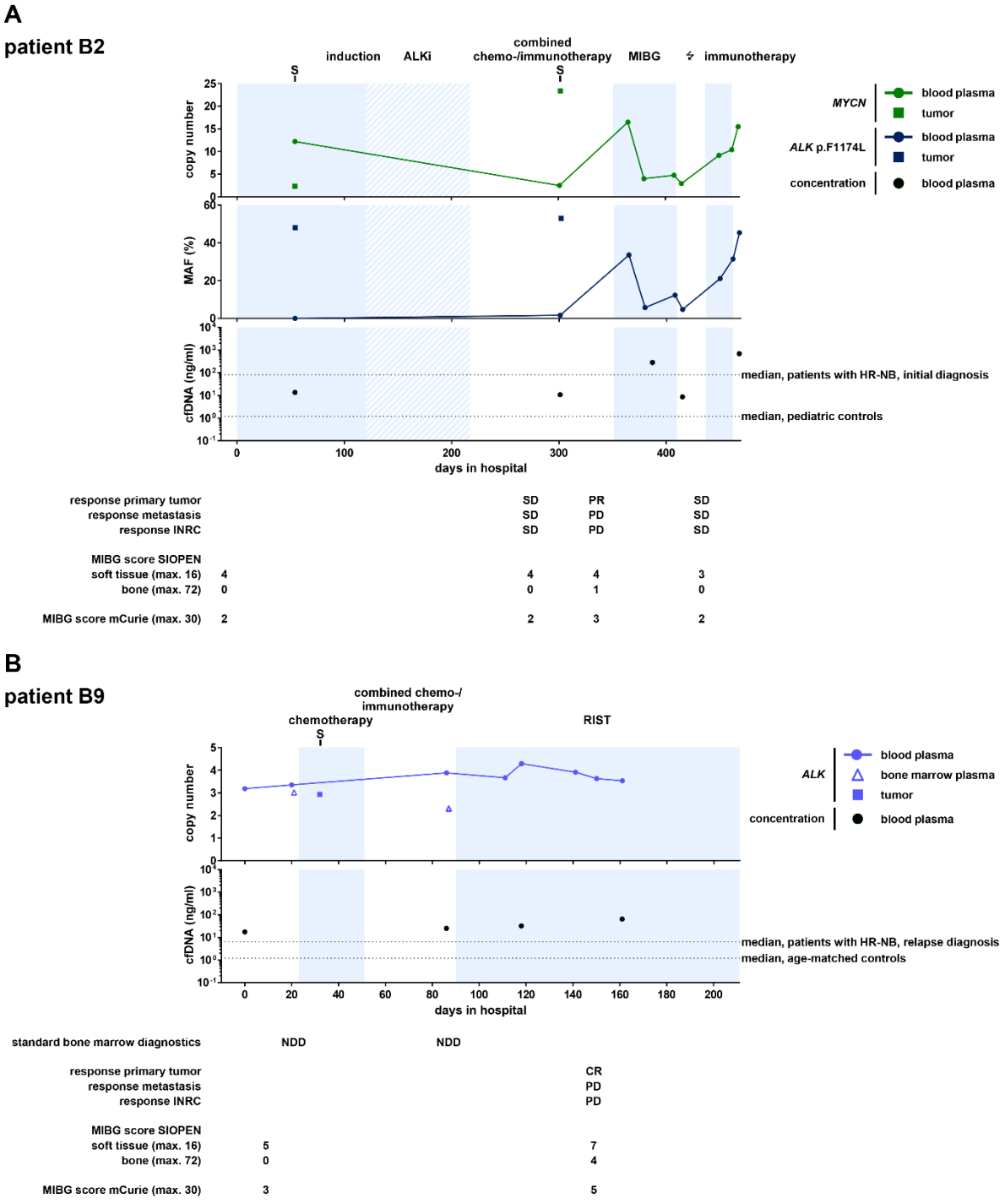

Suppl. Fig. S4. Targeted cfDNA analysis detects intratumor heterogeneity and marker persistence. The graphical display integrates biosample and analysis type along the patient course timeline for *MYCN* (green) and *ALK* (blue) copy numbers and the frequency of the *ALK* p.F1174L mutant allele (dark blue, detected by ddPCR in purified cfDNA and genomic DNA, *upper time line*) as well as total cfDNA concentrations (*lower time line*) and selected clinical case information (*below time lines*). Data are from longitudinally collected samples from patients B2 (**A**) and B9 (**B**). Total cfDNA concentrations in the selected samples were quantified using the Agilent 4200 TapeStation System. Dashed lines indicate the median cfDNA concentrations in the indicated cohorts. Light blue and white backgrounds represent different treatments modules. ALKi, ALK inhibitor treatment; MAF, mutant allele frequency; MIBG, ^{123}I-meta-iodobenzylguanidine therapy; NDD, no detectable disease; RIST, molecularly targeted multimodal approach consisting of metronomic courses of rapamycin/dasatinib and irinotecan/temozolomide; ϟ, radiation; S, surgery. INRC, International Neuroblastoma Response Criteria: CR, complete remission; PD, progressive disease; PR, partial response; SD, stable disease.

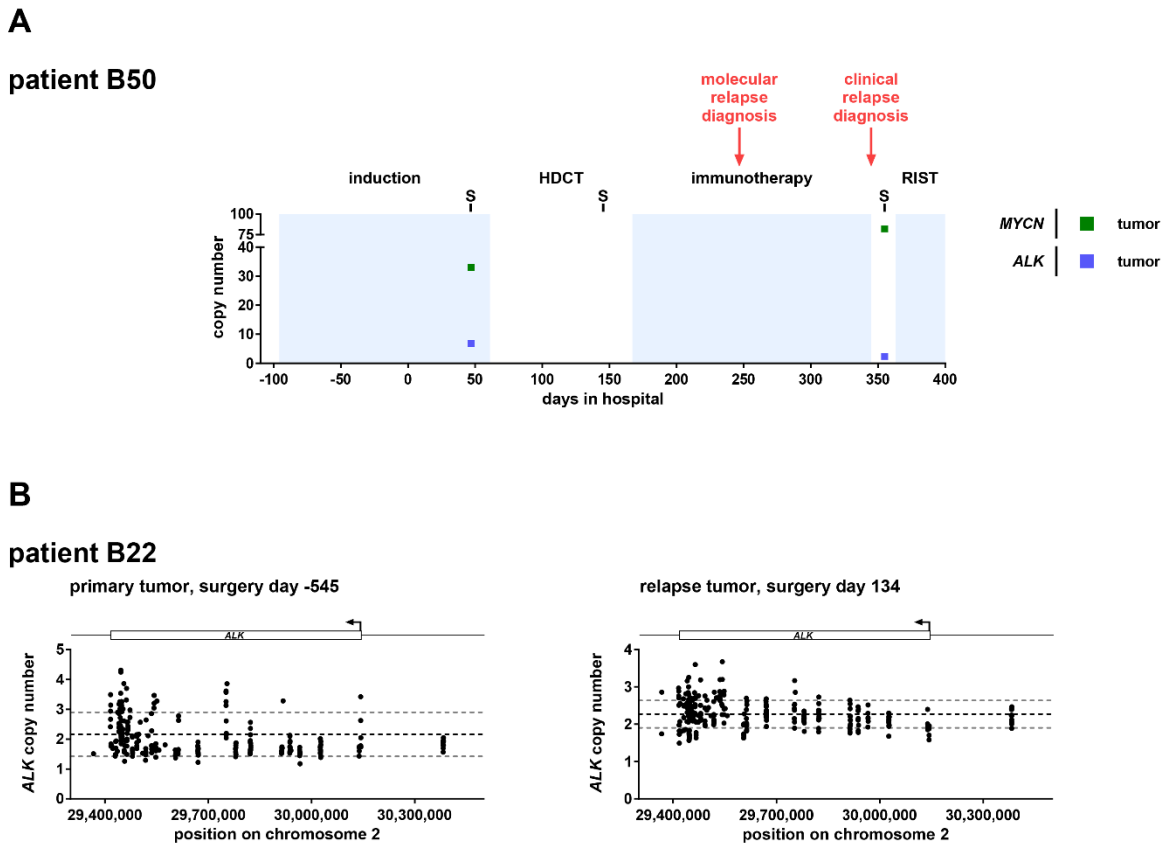

Suppl. Fig. S5. *MYCN* and *ALK* copy number assessment in solid tumor tissue from patients with high-risk neuroblastoma. A, *MYCN (*green) and *ALK* (blue) copy numbers detected by ddPCR in genomic DNA isolated from tumor tissue samples from patient B50 are shown. Light blue and white backgrounds represent different treatments modules. HDCT, high-dose chemotherapy; RIST, molecularly targeted multimodal approach consisting of metronomic courses of rapamycin/dasatinib and irinotecan/temozolomide; S, surgery. *ALK* copy number was assessed by hybrid capture-based panel sequencing in genomic DNA isolated from tissue biopsies of the primary (**B**) and relapse (**C**) tumors arising in patient B22. Detected (called) copy numbers are visualized as dots for the different position along the *ALK* gene on chromosome 2p (indicated above each plot). Bold black dashed line indicates the mean baseline *ALK* copy number with ± SD as grey dashed lines.

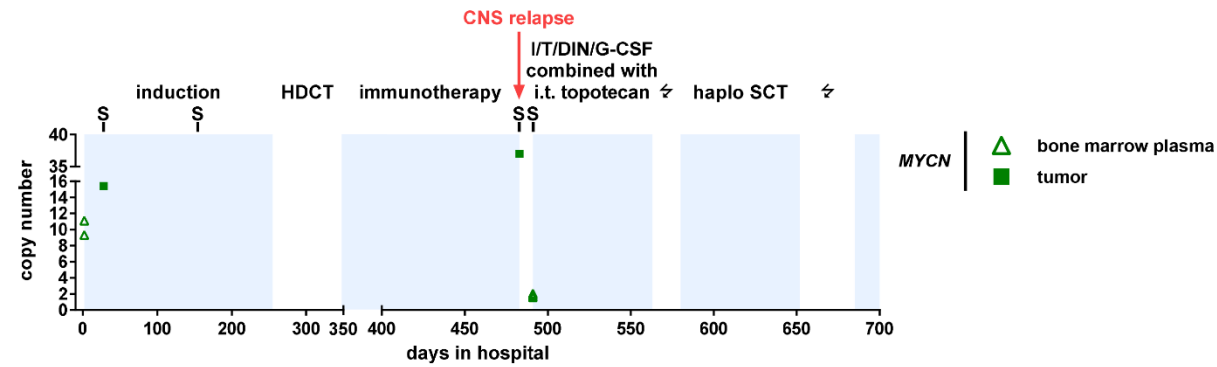

Suppl. Fig. S6. *MYCN* copy number assessed in cfDNA purified from bone marrow samples and genomic DNA purified from tumor tissue samples from patient B35. *MYCN* copy numbers (green) were measured by ddPCR in cfDNA purified from longitudinally collected bone marrow samples and corresponding tumor tissue samples from patient B35. The light blue and white bars represent different treatments modules. CNS, central nervous system; haplo SCT, haploidentical hematopoietic stem cell transplantation, HDCT, high-dose chemotherapy; I/T/DIN/G-CSF, irinotecan/temozolomide/dinutuximab beta/granulocyte colony stimulating factor; i.t., intrathecal; ϟ, radiation; S, surgery.

SUPPLEMENTARY TABLES

Suppl. Table S1. Patient and tumor characteristics in the study population.

Factor	No. of patients	% of study population
Sex		
male	21	67.7
female	10	32.3
Age at diagnosis		
< 18 months	9	29.0
≥ 18 months	22	71.0
MYCN status[1]		
diploid	15	48.4
amplified	16	51.6
1p36 status[2]		
no aberration	17	54.8
aberration	14	45.2
ALK status[3]		
wildtype	17	54.8
gain	2	6.5
mutation	9	29.0
not available	3	9.7
Overall survival status		
alive	18	58.1
succumbed to disease	11	35.5
died of other causes	2	6.5

[1] Genomic copies of the *MYCN* oncogene as analyzed by fluorescence in situ hybridization, Southern blot and hybrid capture-based panel sequencing. *MYCN* amplification was defined as >8 genomic copies.
[2] Genomic status of the chromosome 1p36 region as analyzed by fluorescence in situ hybridization and PCR.
[3] *ALK* status as analyzed by hybrid capture-based panel sequencing.

Suppl. Table S2.

Clinical and molecular genetic covariates in patients with INRG stage M high-risk neuroblastoma as defined by the German NB2004 neuroblastoma trial protocol and 2017 GPOH Guidelines for Diagnosis and Treatment of Patients with Neuroblastic Tumors.

ID#[1]	Age at diagnosis [d][2]	Sex[3]	EFS status[4]	OS status[5]	*MYCN* status[6]	1p36 status[7]	*ALK* status[8]
B1	5145	M	1	1	N	N	N
B2	666	F	1	1	Amp	Aberration	*ALK* p.F1174L
B8	107	M	1	1	Amp	Aberration	N
B9	1435	M	1	1	N	N	n.a.
B10	513	M	0	0	Amp	Aberration	*ALK* p.R1275Q
B11	1885	M	1	1	N	Aberration	N
B12	64	M	1	1	N	N	*ALK* p.R1275Q
B13	306	F	0	0	N	N	N
B15	1743	M	1	1	N	N	*ALK* p.R1275Q
B17	443	F	1	1	Amp	N	*ALK* p.R1275Q
B18	235	M	0	0	Amp	Aberration	N
B19	1012	M	0	0	N	N	*ALK* p.R1231W
B20	727	M	0	0	Amp	Aberration	n.a.
B21	2916	M	1	1	Amp	Aberration	*ALK* p.R1275Q
B22	1544	F	1	0	N	N	Gain
B23	1049	M	0	0	N	N	N
B27	886	M	0	0	N	N	N
B33	824	M	1	1	N	Aberration	n.a.
B35	364	M	1	0	Amp	N	N
B36	2341	M	1	1	N	N	N
B38	1124	F	0	0	Amp	Aberration	*ALK* p.R1275Q
B40	544	F	0	2	Amp	Aberration	N
B42	1395	F	0	0	Amp	Aberration	*ALK* p.F1174L
B48	1130	M	0	2	Amp	Aberration	N
B50	1089	F	1	0	Amp	N	Gain
B54	318	M	0	0	Amp	N	N
B69	2522	M	0	0	N	N	N
B73	984	F	0	0	Amp	N	N
B79	1065	F	0	0	N	N	N
B82	2084	M	0	0	N	Aberration	N
B87	689	M	0	0	Amp	Aberration	N

[1] Patient code
[2] Patient age at diagnosis in days
[3] Patient sex. M = male; F = female
[4] Event-free survival. 0 = no event; 1 = event
[5] Overall survival. 0 = alive; 1 = succumbed to disease; 2 = died of other causes
[6] Genomic copies of the *MYCN* oncogene as analyzed by fluorescence in situ hybridization, Southern blot and hybrid capture-based panel sequencing. AMP = amplified *MYCN* (>8 genomic copies); N = unaltered *MYCN*.
[7] Genomic status of the chromosome 1p36 region as analyzed by fluorescence in situ hybridization and PCR. N = unaltered.
[8] *ALK* status as analyzed by hybrid capture-based panel sequencing. N = unaltered; G = *ALK* gain (3-8 copies); n.a. = not available.

Suppl. Table S3.

Total blood- and bone marrow-derived cfDNA quantities from patients with high-risk neuroblastoma or acute lymphoblastic leukemia and from healthy control individuals.

Study Population	No. of individuals	Sample type	cfDNA [ng]			
			Median	Inter-quartile range	Lowest value	Highest value
pediatric controls	25	blood plasma	0.72	0.36 – 1.23	0.10	1.98
patients with HR-NB[1], initial diagnosis	24		94.75	11.53 – 270.60	0.17	935.00
patients with HR-NB[1], relapse diagnosis	10		16.80	7.91 – 37.63	6.55	128.00
healthy individuals	24	bone marrow plasma	25.25	5.54 – 59.38	0.94	165.00
patients with HR-NB[1] with bone marrow infiltration	16		113.30	45.51 – 255.60	4.46	956.00
patients with ALL[2]	28		10.25	3.76 – 16.85	1.30	199.00

[1] High-risk neuroblastoma
[2] Acute lymphoblastic leukemia

Suppl. Table S4.

Primer and probe sequences and concentrations used in duplex ddPCR protocols to assess *ALK* and *MYCN* copy number status.

Primer/Probe	Sequence (5'-3')	Concentration [nM]
ALK-exon3-intron3-for[1]	AGATGGACTTGCTGGATGGG	900
ALK- exon3-intron3-rev[1]	GCAGCCTCTCCCTTACCTC	900
ALK- exon3-intron3-probe[1]	FAM-GGCAGAGCGTTCTAAGGAGA-BHQ1	250
ALK-intron8-exon9-for[2]	CTTGTCCTCTGACTCTTCTCG	900
ALK-intron8-exon9-rev[2]	CAAGACTCCACGAATGAGC	900
ALK-intron8-exon9-probe[2]	FAM-TCACAGCTCCGAATGTCCTG-BHQ1	250
MYCN-for[3]	GTGCTCTCCAATTCTCGCCT	900
MYCN-rev[3]	GATGGCCTAGAGGAGGGCT	900
MYCN-probe[3]	FAM-CACTAAAGTTCCTTCCACCCTCTCCT-BHQ1	250
NAGK-for[3]	TGGGCAGACACATCGTAGCA	900
NAGK-rev[3]	CACCTTCACTCCCACCTCAAC	900
NAGK-probe[3]	HEX-TGTTGCCCGAGATTGACCCGGT-BHQ1	250

[1] Amplicon position: chr2:29694834-29694903 (NM_004304.5; strand:-; GRCh38/hg38) (3)

[2] Amplicon position: chr2:29297025-29297087 (NM_004304.5; strand:-; GRCh38/hg38) (4)

[3] Adapted from Gotoh et al., 2005 (5)

Suppl. Table S5.

Primer and probe sequences and concentrations used in duplex ddPCR protocols to detect the neuroblastoma-specific *ALK* p.F1174L and *ALK* p.R1275Q hotspot mutations.

Primer/Probe	Sequence (5'-3')[1]	Concentration [nM]
ALK^{1174}-for	GCCCAGACTCAGCTCAGT	900
ALK^{1174}-rev	CCCCAATGCAGCGAACAAT	900
ALK^{F1174L} probe	FAM-TCTCTGCTCTGCAGCAAATTAAACC-BHQ1	250
ALK^{1174} probe	HEX-TCTCTGCTCTGCAGCAAATTCAACC-BHQ1	250
ALK^{1275}-for	GTCCAGGCCCTGGAAGAG	900
ALK^{1275}-rev	GGGGTGAGGCAGTCTTTACTC	900
ALK^{R1275Q} probe	FAM-TTCGGGATGGCCCAAGACAT-BHQ1	250
ALK^{1275} probe	HEX-TTCGGGATGGCCCGAGACAT-BHQ1	250

[1] Adapted from Combaret et al., 2015 (6)

Suppl. Table S6.

Comparative analysis of molecular marker profiles in paired blood/tumor tissue samples from patients with high-risk neuroblastoma.

Time point	Sample type	No. of matched sample pairs	Overlap of marker expression in paired blood/tumor tissue samples (%)			
			MYCN CN[1]	*ALK* CN[1]	*ALK* p.F1174L	*ALK* p.R1275Q
initial diagnosis	biopsy	14	85.7	35.7	92.9	85.7
initial diagnosis	resection	14	71.4	42.9	92.9	92.9
relapse	biopsy	6	83.3	66.7	100*	83.3
relapse	resection	1	0	100	100	100

[1] CN, copy number

* Frequency of the *ALK* p.F1174L mutant allele was compared in n=5 paired blood/tumor biopsy samples.

Suppl. Table S7.

Overview of *MYCN* and *ALK* copy numbers detected by ddPCR in longitudinally collected biosamples from patient B50.

Days in hospital	*MYCN* copy number			*ALK* copy number		
	Blood plasma	Bone marrow plasma[1]	Tumor	Blood plasma	Bone marrow plasma[1]	Tumor
0	2.20			2.20		
9		1.84			1.99	
		1.90			2.10	
		1.96			2.87	
		1.65			1.92	
21	1.75			1.87		
47			33.0			6.80
48	1.86			2.44		
69	3.70			3.90		
173	1.40			1.70		
180	1.70			2.90		
247	6.10			2.60		
349	14.8	11.4		2.74	2.18	
		9.60			2.20	
		6.10			2.10	
		6.70			2.25	
355			82.0			2.35
364	25.8			1.95		
594	2.09			2.19		
742	1.97			2.20		

[1] Bone marrow samples were obtained from different locations.

Suppl. Table S8.

Overview of *MYCN* copy number detected by ddPCR in longitudinally collected biosamples from patient B82.

Days in hospital	*MYCN* copy number	
	Blood plasma	Tumor
1	2.08	3.11
142		1.74

Suppl. Table S9.

Overview of *MYCN* copy number and *ALK* p.F1174L mutant allele frequency detected by ddPCR in longitudinally collected biosamples from patient B2.

Days in hospital	*MYCN* copy number		*ALK* p.F1174L MAF (%)[1]		
	Blood plasma	Tumor	Blood plasma	Tumor	Germline
54	12.2	2.33	0	48.0	
301	2.48		1.70		0
302		23.4		53.0	
365	16.5		33.6		
380	4.00		5.80		
408	4.77		12.3		
415	2.92		4.80		
450	9.14		21.1		
462	10.4		31.5		
468	15.5		45.4		

[1] Mutant allele frequency (MAF) of 0% indicates wildtype *ALK*.

Suppl. Table S10.

Overview of *ALK* copy number detected by ddPCR in longitudinally collected biosamples from patient B22.

Days in hospital	*ALK* copy number	
	Blood plasma	Bone marrow plasma[1]
0	2.10	
10	2.87	
132	3.11	
134		2.34
		2.24
		2.98
		2.10
358	2.00	
445	2.27	
1062	2.04	

[1] Bone marrow samples were obtained from different locations.

Suppl. Table S11.

Overview of *MYCN* copy number and *ALK* p.R1275Q mutant allele frequency detected by ddPCR in longitudinally collected biosamples from patient B10.

Days in hospital	*MYCN* copy number			*ALK* p.R1275Q MAF (%)[2]			
	Blood plasma	Bone marrow plasma[1]	Tumor	Blood plasma	Bone marrow plasma[1]	Tumor	Germline
0	35.0			28.9			0
1		79.5	193.9		30.8	48.2	
39	2.60	2.93		0	0		
		2.64			0		
59	2.07			0			
60		1.92			0		
		1.94			0		
114	1.70			0			
115			24.27			1.22	
162	1.63			0			
254	1.33			0			
261	1.55			0			
375	1.93			0			
840	1.60			0			
889	2.00			0			
1036	2.30			0			
1141	1.60			0			

[1] Bone marrow samples were obtained from different locations.
[2] Mutant allele frequency (MAF) of 0% indicates wildtype *ALK*.

Suppl. Table S12.

Overview of *MYCN* copy number and frequencies of *ALK* p.F1174L and *ALK* p.R1275Q mutant alleles detected by ddPCR in longitudinally collected biosamples from patient B42.

Days in hospital	*MYCN* copy number			*ALK* p.F1174L MAF (%)[2]				*ALK* p.R1275Q MAF (%)[2]			
	Blood plasma	Bone marrow plasma[1]	Tumor	Blood plasma	Bone marrow plasma[1]	Tumor	Germline	Blood plasma	Bone marrow plasma[1]	Tumor	Germline
0	59.5			36.8				0			
1	67.5	25.5	28.69	36.2	5.70	12.95	0	0.20	0	0	0
		20.9			10.8				0.35		
		18.7			6.70				0		
		27.5			10.2				0.60		
12	40.0			35.2				0			
22	3.90			1.70				0			
28	4.40			1.70				0			
48		2.42			0				0		
		2.02			0				0		
		1.86			0				0		
		2.02			0				0		
54	3.30			4.40				0			
78	1.84			0				0			
119	1.80[3]			0				0			
	1.86[4]		20.2	0.15		18.9		0		0	
137	1.76			0				0			
160		1.81			0				0		
		2.20			0				0		
		1.89			0				0		
		1.93			0				0		
181	1.90[3]			0				0			
	2.36[4]		6.50	0		3.90		0		0	
237	2.06			0				0			
256	1.60			0				0			
316	1.80			0				0			
329	1.65			0				0			
386	1.73			0				0			

[1] Bone marrow samples obtained from different localizations
[2] Mutant allele frequency (MAF) of 0% indicates wildtype *ALK*.
[3] Sample collection prior to surgery
[4] Sample collection within 12 hours post-surgery

Suppl. Table S13.

Overview of *ALK* copy number detected by ddPCR in longitudinally collected biosamples from patient B9.

Days in hospital	*ALK* copy number		
	Blood plasma	Bone marrow plasma[1]	Tumor
0	3.18		
20	3.35		
21		3.02	
32			2.93
86	3.88		
87		2.29	
		2.32	
111	3.66		
118	4.29		
141	3.91		
150	3.63		
161	3.53		

[1] Bone marrow samples were obtained from different locations

Suppl. Table S14.

Overview of *MYCN* copy number detected by ddPCR in longitudinally collected biosamples from patient B35.

Days in hospital	*MYCN* copy number			
	Blood plasma	Bone marrow plasma[1]	Cerebrospinal fluid	Tumor
0	21.1			
2		11.1		
		9.30		
28	3.90			15.4
34	3.35			
59	2.13			
85	2.29			
98	1.90			
179	2.60			
267	1.44			
417	1.61			
483				37.0
487	4.20			
491	2.47	1.83	10.9	
		2.04		
		1.58		
		1.77		
498	1.80	4.80	4.80	
501	1.70			
505	1.70	2.80	2.80	
512	2.10	1.95	1.95	
540	1.90			
547		2.40	2.40	
566	1.70			
607			ND	
621	1.90			
697	1.88		ND	

[1] Bone marrow samples were obtained from different locations.
ND, not detectable

SUPPLEMENTARY REFERENCES

1. Szymansky A, Kruetzfeldt LM, Heukamp LC, Hertwig F, Theissen J, Deubzer HE, et al. Neuroblastoma risk assessment and treatment stratification with hybrid capture-based panel sequencing. J Pers Med. 2021;11(8):691.
2. Muller JN, Falk M, Talwar J, Neemann N, Mariotti E, Bertrand M, et al. Concordance between comprehensive cancer genome profiling in plasma and tumor specimens. J Thorac Oncol. 2017;12(10):1503-1511.
3. Lodrini M, Sprussel A, Astrahantseff K, Tiburtius D, Konschak R, Lode HN, et al. Using droplet digital PCR to analyze MYCN and ALK copy number in plasma from patients with neuroblastoma. Oncotarget. 2017;8(49):85234-85251.
4. Peitz C, Sprussel A, Linke RB, Astrahantseff K, Grimaldi M, Schmelz K, et al. Multiplexed quantification of four neuroblastoma DNA targets in a single droplet digital PCR reaction. J Mol Diagn. 2020;S1525-1578(20)30446-3.
5. Gotoh T, Hosoi H, Iehara T, Kuwahara Y, Osone S, Tsuchiya K, et al. Prediction of MYCN amplification in neuroblastoma using serum DNA and real-time quantitative polymerase chain reaction. J Clin Oncol. 2005;23(22):5205-10.
6. Combaret V, Iacono I, Bellini A, Brejon S, Bernard V, Marabelle A, et al. Detection of tumor ALK status in neuroblastoma patients using peripheral blood. Cancer Med. 2015;4(4):540-50.